

Fundamental Matrix Computation: Theory and Practice

Kenichi KANATANI*

Department of Computer Science
Okayama University
Okayama 700-8530 Japan

Yasuyuki SUGAYA

Department of Information and Computer Sciences
Toyohashi University of Technology
Toyohashi, Aichi 441-8580 Japan

(Received November 14, 2007)

We classify and review existing algorithms for computing the fundamental matrix from point correspondences and propose new effective schemes: 7-parameter Levenberg-Marquardt (LM) search, EFNS, and EFNS-based bundle adjustment. Doing experimental comparison, we show that EFNS and the 7-parameter LM search exhibit the best performance and that additional bundle adjustment does not increase the accuracy to any noticeable degree.

1. Introduction

Computing the fundamental matrix from point correspondences is the first step of many vision applications including camera calibration, image rectification, structure from motion, and new view generation [7]. Fundamental matrix computation has attracted a special attention because of the following two characteristics:

1. Feature points are extracted by an image processing operation [8, 17, 20, 23]. As a result, the detected locations invariably have uncertainty to some degree.
2. Detected points are matched by comparing surrounding regions in respective images, using various measures of similarity and correlation [15, 19, 27]. However, mismatches are unavoidable to some degree.

The first issue has been dealt with by *statistical optimization* [10]: we model the uncertainty as “noise” obeying a certain probability distribution and compute a fundamental matrix such that its deviation from the true value is as small as possible in expectation. The second issue has been coped with by *robust estimation* [21], which can be viewed as hypothesis testing: we compute a tentative fundamental matrix as a hypothesis and check how many points support it. Those points regarded as “abnormal” according to the hypothesis are called *outliers*, otherwise *inliers*, and we look for a fundamental matrix that has as many inliers as possible.

Thus, the two issues are inseparably interwoven. In this paper, we focus on the first issue, assuming that all corresponding points are inliers. Such a study

*E-mail kanatani@suri.it.okayama-u.ac.jp

is indispensable for any robust estimation technique to work successfully. However, there is an additional complication in doing statistical optimization of the fundamental matrix: it is constrained to have rank 2, i.e., its determinant is 0. This rank constraint has been incorporated in various ways. Here, we categorize them into the following three approaches:

A posteriori correction

The fundamental matrix is optimally computed without considering the rank constraint and is modified in an optimal manner so that the constraint is satisfied (Fig. 1(a)).

Internal access

The fundamental matrix is minimally parameterized so that the rank constraint is identically satisfied and is optimized in the reduced (“internal”) parameter space (Fig. 1(b)).

External access

We do iterations in the redundant (“external”) parameter space in such a way that an optimal solution that satisfies the constraint automatically results (Fig. 1(c)).

In this paper, we review existing methods in this framework and propose new methods. The originality of this paper is in the following four points:

1. We present a new 7-parameter LM search technique as an internal access method¹.
2. We present a new external access method called “EFNS”².

¹A preliminary version was presented in our conference paper [24].²A preliminary version was presented in a more abstract form in our conference paper [14].

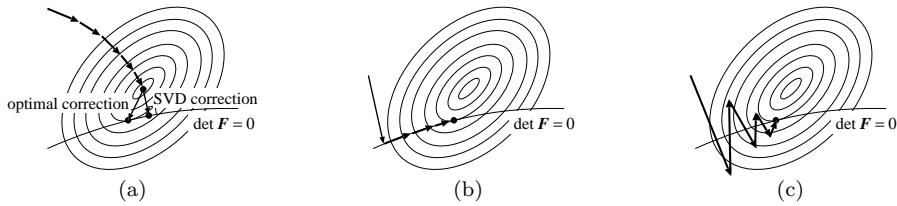


Figure 1: (a) A posteriori correction. (b) Internal access. (c) External access.

3. We present a new compact bundle adjustment algorithm involving the fundamental matrix alone using EFNS³.
4. We experimentally compare the performance of existing and proposed methods by doing numerical experiments using simulated and real images⁴.

In Section 2, we summarize the mathematical background. In Section 3, we study the a posteriori correction approach. We review two correction schemes (SVD correction and optimal correction), three unconstrained optimization techniques (FNS, HEIV, projective Gauss-Newton iterations), and two initialization methods (least squares (LS) and the Taubin method). In Section 4, we focus on the internal access approach and present a compact scheme for doing 7-parameter Levenberg-Marquardt (LM) search. In Section 5, we investigate the external access approach and point out that the CFNS of Chojnacki et al. [4], a pioneering external access method, does not necessarily converge to a correct solution. To complement this, we present a new method called EFNS and demonstrate that it always converges to an optimal value; a mathematical justification is given to this. In Section 6, we compare the accuracy of all the methods and conclude that our EFNS and the 7-parameter LM search started from optimally corrected ML exhibit the best performance. In Section 7, we study the bundle adjustment (Gold Standard) approach and present a new efficient computational scheme for it. In Section 8, we experimentally test the effect of this approach and conclude that additional bundle adjustment does not increase the accuracy to any noticeable degree. Section 9 concludes this paper.

2. Mathematical Fundamentals

Fundamental matrix. We are given two images of the same scene. We take the image origin $(0, 0)$ at the frame center. Suppose a point (x, y) in the first image corresponds to (x', y') in the second. We

³This has not been published anywhere yet.

⁴Part of the numerical results were shown in our conference paper [25], but the EFNS-based bundle adjustment was not included there.

represent them by 3-D vectors

$$\mathbf{x} = \begin{pmatrix} x/f_0 \\ y/f_0 \\ 1 \end{pmatrix}, \quad \mathbf{x}' = \begin{pmatrix} x'/f_0 \\ y'/f_0 \\ 1 \end{pmatrix}, \quad (1)$$

where f_0 is a scaling constant of the order of the image size⁵. As is well known, \mathbf{x} and \mathbf{x}' satisfy the *epipolar equation* [7],

$$(\mathbf{x}, \mathbf{F}\mathbf{x}') = 0, \quad (2)$$

where and hereafter we denote the inner product of vectors \mathbf{a} and \mathbf{b} by (\mathbf{a}, \mathbf{b}) . The matrix $\mathbf{F} = (F_{ij})$ in (2) is of rank 2 and called the *fundamental matrix*; it depends on the relative positions and orientations of the two cameras and their intrinsic parameters (e.g., their focal lengths) but not on the scene or the choice of the corresponding points. If we define⁶

$$\mathbf{u} = (F_{11}, F_{12}, F_{13}, F_{21}, F_{22}, F_{23}, F_{31}, F_{32}, F_{33})^\top, \quad (3)$$

$$\boldsymbol{\xi} = (xx', xy', xf_0, yx', yy', yf_0, f_0x', f_0y', f_0^2)^\top, \quad (4)$$

we can rewrite (2) as

$$(\mathbf{u}, \boldsymbol{\xi}) = 0. \quad (5)$$

The magnitude of \mathbf{u} is indeterminate, so we normalize it to $\|\mathbf{u}\| = 1$, which is equivalent to scaling \mathbf{F} so that $\|\mathbf{F}\| = 1$ ⁷. With a slight abuse of symbolism, we hereafter denote by “ $\det \mathbf{u}$ ” the determinant of the matrix \mathbf{F} defined by \mathbf{u} . If we write N observed noisy correspondence pairs as 9-D vectors $\{\boldsymbol{\xi}_\alpha\}$ in the form (4), our task is to estimate from $\{\boldsymbol{\xi}_\alpha\}$ a 9-D vector \mathbf{u} that satisfies (5) subject to the constraints $\|\mathbf{u}\| = 1$ and $\det \mathbf{u} = 0$.

Covariance matrices. Let us write $\boldsymbol{\xi}_\alpha = \bar{\boldsymbol{\xi}}_\alpha + \Delta\boldsymbol{\xi}_\alpha$, where $\bar{\boldsymbol{\xi}}_\alpha$ is the true value and $\Delta\boldsymbol{\xi}_\alpha$ the noise term. The covariance matrix of $\boldsymbol{\xi}_\alpha$ is defined by

$$V[\boldsymbol{\xi}_\alpha] = E[\Delta\boldsymbol{\xi}_\alpha \Delta\boldsymbol{\xi}_\alpha^\top], \quad (6)$$

where $E[\cdot]$ denotes expectation over the noise distribution. If the noise in the x - and y -coordinates is

⁵This is for stabilizing numerical computation [6]. In our experiments, we set $f_0 = 600$ pixels.

⁶The vector $\boldsymbol{\xi}$ is known as the “Kronecker product” of the vectors $(x, y, f_0)^\top$ and $(x', y', f_0)^\top$.

⁷In this paper, we use the Euclidean (or l_2) norm for vectors and the Frobenius norm for matrices.

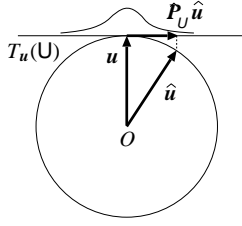


Figure 2: The deviation is projected onto the tangent space, with which we identify the noise domain.

independent and has mean 0 and standard deviation σ , the covariance matrix of ξ_α has the form $V[\xi_\alpha] = \sigma^2 V_0[\xi_\alpha]$ up to $O(\sigma^4)$, where

$$V_0[\xi_\alpha] = \begin{pmatrix} \bar{x}_\alpha^2 + \bar{x}'_\alpha{}^2 & \bar{x}_\alpha \bar{y}'_\alpha & f_0 \bar{x}'_\alpha & \bar{x}_\alpha \bar{y}_\alpha & 0 & 0 & 0 & 0 & 0 & 0 \\ \bar{x}'_\alpha \bar{y}'_\alpha & \bar{x}_\alpha^2 + \bar{y}'_\alpha{}^2 & f_0 \bar{y}'_\alpha & 0 & 0 & 0 & 0 & 0 & 0 & 0 \\ f_0 \bar{x}'_\alpha & f_0 \bar{y}'_\alpha & f_0^2 & 0 & 0 & 0 & 0 & 0 & 0 & 0 \\ \bar{x}_\alpha \bar{y}_\alpha & 0 & 0 & \bar{y}_\alpha^2 + \bar{x}'_\alpha{}^2 & 0 & 0 & 0 & 0 & 0 & 0 \\ 0 & \bar{x}_\alpha \bar{y}_\alpha & 0 & \bar{x}'_\alpha \bar{y}'_\alpha & 0 & 0 & 0 & 0 & 0 & 0 \\ 0 & 0 & 0 & f_0 \bar{x}'_\alpha & 0 & 0 & 0 & 0 & 0 & 0 \\ f_0 \bar{x}_\alpha & 0 & 0 & f_0 \bar{y}_\alpha & 0 & 0 & 0 & 0 & 0 & 0 \\ 0 & f_0 \bar{x}_\alpha & 0 & 0 & 0 & 0 & 0 & 0 & 0 & 0 \\ 0 & 0 & 0 & 0 & 0 & 0 & 0 & 0 & 0 & 0 \\ 0 & 0 & f_0 \bar{x}_\alpha & 0 & 0 & 0 & 0 & 0 & 0 & 0 \\ \bar{x}_\alpha \bar{y}_\alpha & 0 & 0 & f_0 \bar{x}_\alpha & 0 & 0 & 0 & 0 & 0 & 0 \\ 0 & 0 & 0 & 0 & 0 & 0 & 0 & 0 & 0 & 0 \\ \bar{x}'_\alpha \bar{y}'_\alpha & f_0 \bar{x}'_\alpha & f_0 \bar{y}_\alpha & 0 & 0 & 0 & 0 & 0 & 0 & 0 \\ \bar{y}_\alpha^2 + \bar{y}'_\alpha{}^2 & f_0 \bar{y}'_\alpha & 0 & f_0 \bar{y}_\alpha & 0 & 0 & 0 & 0 & 0 & 0 \\ f_0 \bar{y}'_\alpha & f_0^2 & 0 & 0 & 0 & 0 & 0 & 0 & 0 & 0 \\ 0 & 0 & f_0^2 & 0 & 0 & 0 & 0 & 0 & 0 & 0 \\ f_0 \bar{y}_\alpha & 0 & 0 & f_0^2 & 0 & 0 & 0 & 0 & 0 & 0 \\ 0 & 0 & 0 & 0 & 0 & 0 & 0 & 0 & 0 & 0 \end{pmatrix}. \quad (7)$$

In actual computation, the true positions $(\bar{x}_\alpha, \bar{y}_\alpha)$ and $(\bar{x}'_\alpha, \bar{y}'_\alpha)$ are replaced by their data (x_α, y_α) and (x'_α, y'_α) , respectively⁸.

We define the covariance matrix $V[\hat{\mathbf{u}}]$ of the resulting estimate $\hat{\mathbf{u}}$ of \mathbf{u} by

$$V[\hat{\mathbf{u}}] = E[(\mathbf{P}_U \hat{\mathbf{u}})(\mathbf{P}_U \hat{\mathbf{u}})^\top], \quad (8)$$

where \mathbf{P}_U is the linear operator projecting \mathcal{R}^9 onto the domain \mathcal{U} of \mathbf{u} defined by the constraints $\|\mathbf{u}\| = 1$ and $\det \mathbf{u} = 0$; we evaluate the error of $\hat{\mathbf{u}}$ by projecting it onto the tangent space $T_{\mathbf{u}}(\mathcal{U})$ to \mathcal{U} at \mathbf{u} (Fig. 2) [10, 12].

Geometry of the constraint. The unit normal to the hypersurface defined by $\det \mathbf{u} = 0$ is given by

⁸Experiments have confirmed that this does not noticeable changes in final results.

$\nabla_{\mathbf{u}} \det \mathbf{u}$. After normalization, it has the form

$$\mathbf{u}^\dagger \equiv \mathbf{N} \begin{bmatrix} u_5 u_9 - u_8 u_6 \\ u_6 u_7 - u_9 u_4 \\ u_4 u_8 - u_7 u_5 \\ u_8 u_3 - u_2 u_9 \\ u_9 u_1 - u_3 u_7 \\ u_7 u_2 - u_1 u_8 \\ u_2 u_6 - u_5 u_3 \\ u_3 u_4 - u_6 u_1 \\ u_1 u_5 - u_4 u_2 \end{bmatrix}, \quad (9)$$

where $\mathbf{N}[\cdot]$ denotes normalization into unit norm. Since the inside of $\mathbf{N}[\cdot]$ represents the ‘‘cofactor’’ of \mathbf{F} in the vector form of (3), we call \mathbf{u}^\dagger , the *cofactor vector* of \mathbf{u} . It is easily seen that the rank constraint $\det \mathbf{u} = 0$ is equivalently written as⁹

$$(\mathbf{u}^\dagger, \mathbf{u}) = 0. \quad (10)$$

Since \mathbf{u} is orthogonal to the unit sphere $\mathcal{S}^8 \subset \mathcal{R}^9$ and since the domain \mathcal{U} is included in \mathcal{S}^8 , the vector \mathbf{u} is everywhere orthogonal to \mathcal{U} . On the other hand, the cofactor vector \mathbf{u}^\dagger is orthogonal to the hypersurface defined by $\det \mathbf{u} = 0$ and hence is orthogonal to \mathcal{U} which is included in that hypersurface. Together with (10), we see that $\{\mathbf{u}, \mathbf{u}^\dagger\}$ is an orthonormal basis of the orthogonal complement of the tangent space $T_{\mathbf{u}}(\mathcal{U})$. It follows that the projection operator \mathbf{P}_U in (8) has the following matrix representation:

$$\mathbf{P}_U = \mathbf{I} - \mathbf{u} \mathbf{u}^\top - \mathbf{u}^\dagger \mathbf{u}^{\dagger\top}. \quad (11)$$

KCR lower bound. If the noise in $\{\xi_\alpha\}$ is independent and Gaussian with mean $\mathbf{0}$ and covariance matrix $\sigma^2 V_0[\xi]$, the following inequality holds for an arbitrary unbiased estimator $\hat{\mathbf{u}}$ of \mathbf{u} [10, 12]:

$$V[\hat{\mathbf{u}}] \succ \sigma^2 \left(\sum_{\alpha=1}^N \frac{(\mathbf{P}_U \bar{\xi}_\alpha)(\mathbf{P}_U \bar{\xi}_\alpha)^\top}{(\mathbf{u}, V_0[\xi_\alpha] \mathbf{u})} \right)_s^-. \quad (12)$$

Here, \succ means that the left-hand side minus the right is positive semidefinite, and $(\cdot)_r^-$ denotes the pseudoinverse of rank r . Chernov and Lesort [2] called the right-hand side of (12) the *KCR (Kanatani-Cramer-Rao) lower bound* and showed that (12) holds up to $O(\sigma^4)$ even if $\hat{\mathbf{u}}$ is not unbiased; it is sufficient that $\hat{\mathbf{u}} \rightarrow \mathbf{u}$ as $\sigma \rightarrow 0$ [2].

Maximum likelihood. If the noise in $\{\xi_\alpha\}$ is independent and Gaussian with mean $\mathbf{0}$ and covariance matrix $\sigma^2 V_0[\xi]$, *maximum likelihood (ML)* estimation of \mathbf{u} is to minimize the sum of square Mahalanobis distances

⁹This is also a consequence of the well known identity $\mathbf{F}^\dagger \mathbf{F} = (\det \mathbf{F}) \mathbf{I}$.

$$J = \sum_{\alpha=1}^N (\boldsymbol{\xi}_\alpha - \bar{\boldsymbol{\xi}}_\alpha, V_0[\boldsymbol{\xi}_\alpha]_4^-(\boldsymbol{\xi}_\alpha - \bar{\boldsymbol{\xi}}_\alpha)), \quad (13)$$

subject to $(\mathbf{u}, \bar{\boldsymbol{\xi}}_\alpha) = 0$, $\alpha = 1, \dots, N$. Geometrically, we are fitting a hyperplane $(\mathbf{u}, \boldsymbol{\xi}) = 0$ in the $\boldsymbol{\xi}$ -space to N points $\{\boldsymbol{\xi}_\alpha\}$ as closely as possible; the closeness is measured in the Mahalanobis distance, the distance weighted by the $-1/2$ th power of the covariance matrix $V_0[\boldsymbol{\xi}_\alpha]$ representing the uncertainty of each datum.

Eliminating the constraints $(\mathbf{u}, \bar{\boldsymbol{\xi}}_\alpha) = 0$ by using Lagrange multipliers, we obtain [10, 12]

$$J = \sum_{\alpha=1}^N \frac{(\mathbf{u}, \boldsymbol{\xi}_\alpha)^2}{(\mathbf{u}, V_0[\boldsymbol{\xi}_\alpha]\mathbf{u})}. \quad (14)$$

The ML estimator $\hat{\mathbf{u}}$ minimizes this subject to the normalization $\|\mathbf{u}\| = 1$ and the rank constraint $(\mathbf{u}^\dagger, \mathbf{u}) = 0$.

3. A Posteriori Correction

3.1 Correction schemes

The a posteriori correction approach first minimizes (14) without considering the rank constraint and then modifies the resulting solution $\tilde{\mathbf{u}}$ so as to satisfy it (Fig. 1(a)).

SVD correction. A naive idea is to compute the singular value decomposition (SVD) of the computed fundamental matrix and replace the smallest singular value by 0, resulting in a matrix of rank 2 “closest” in the Frobenius norm [6]. We call this *SVD correction*.

Optimal correction. A more sophisticated method is the *optimal correction* [10, 18]. According to the statistical optimization theory [10], the covariance matrix $V[\tilde{\mathbf{u}}]$ of the rank unconstrained solution $\tilde{\mathbf{u}}$ can be evaluated, so $\tilde{\mathbf{u}}$ is moved in the direction of the mostly likely fluctuation implied by $V[\tilde{\mathbf{u}}]$ until it satisfies the rank constraint (Fig. 1(a)). The procedure goes as follows [10]:

1. Compute the following 9×9 matrix $\tilde{\mathbf{M}}$:

$$\tilde{\mathbf{M}} = \sum_{\alpha=1}^N \frac{\boldsymbol{\xi}_\alpha \boldsymbol{\xi}_\alpha^\top}{(\tilde{\mathbf{u}}, V_0[\boldsymbol{\xi}_\alpha]\tilde{\mathbf{u}})}. \quad (15)$$

2. Compute the matrix $V_0[\tilde{\mathbf{u}}]$ as follows:

$$V_0[\tilde{\mathbf{u}}] = \tilde{\mathbf{M}}_8^-. \quad (16)$$

3. Update the solution $\tilde{\mathbf{u}}$ as follows ($\tilde{\mathbf{u}}^\dagger$ is the co-factor vector of $\tilde{\mathbf{u}}$):

$$\tilde{\mathbf{u}} \leftarrow N[\tilde{\mathbf{u}} - \frac{1}{3} \frac{(\tilde{\mathbf{u}}, \tilde{\mathbf{u}}^\dagger) V_0[\tilde{\mathbf{u}}] \tilde{\mathbf{u}}^\dagger}{(\tilde{\mathbf{u}}^\dagger, V_0[\tilde{\mathbf{u}}] \tilde{\mathbf{u}}^\dagger)}]. \quad (17)$$

4. If $(\tilde{\mathbf{u}}, \tilde{\mathbf{u}}^\dagger) \approx 0$, return $\tilde{\mathbf{u}}$ and stop. Else, update the matrix $V_0[\tilde{\mathbf{u}}]$ in the form

$$\mathbf{P}_{\tilde{\mathbf{u}}} = \mathbf{I} - \tilde{\mathbf{u}} \tilde{\mathbf{u}}^\top, \quad V_0[\tilde{\mathbf{u}}] \leftarrow \mathbf{P}_{\tilde{\mathbf{u}}} V_0[\tilde{\mathbf{u}}] \mathbf{P}_{\tilde{\mathbf{u}}}, \quad (18)$$

and go back to Step 3.

Explanation. Since $\tilde{\mathbf{u}}$ is a unit vector, its endpoint is on the unit sphere \mathcal{S}^8 in \mathcal{R}^9 . Essentially, (17) is the Newton iteration formula for displacing $\tilde{\mathbf{u}}$ in the direction in the tangent space $T_{\tilde{\mathbf{u}}}(\mathcal{S}^8)$ along which J is least increased so that $(\tilde{\mathbf{u}}^\dagger, \tilde{\mathbf{u}}) = 0$ is satisfied. However, $\tilde{\mathbf{u}}$ deviates from \mathcal{S}^8 by a high order small distance as it proceeds in $T_{\tilde{\mathbf{u}}}(\mathcal{S}^8)$, so we “pull” it back onto \mathcal{S}^8 using the operator $N[\cdot]$. From that point, the same procedure is repeated until $(\tilde{\mathbf{u}}^\dagger, \tilde{\mathbf{u}}) = 0$. However, the normalized covariance matrix $V_0[\tilde{\mathbf{u}}]$ is defined in the tangent space $T_{\tilde{\mathbf{u}}}(\mathcal{S}^8)$, which changes as $\tilde{\mathbf{u}}$ moves. So, (18) corrects it so that $V_0[\tilde{\mathbf{u}}]$ has the domain $T_{\tilde{\mathbf{u}}}(\mathcal{S}^8)$ at the displaced point $\tilde{\mathbf{u}}$.

3.2 Unconstrained ML

Before imposing the rank constraint, we need to do unconstrained minimization of (14), for which many methods exist including FNS [3], HEIV [16], and the projective Gauss-Newton iterations [13]. Their convergence properties were studied in [13].

FNS. The *FNS* (*Fundamental Numerical Scheme*) of Chojnacki et al. [3] is based on the fact that the derivative of (14) with respect to \mathbf{u} has the form

$$\nabla_{\mathbf{u}} J = 2\mathbf{X}\mathbf{u}, \quad (19)$$

where \mathbf{X} has the following form [3]:

$$\mathbf{X} = \mathbf{M} - \mathbf{L}, \quad (20)$$

$$\mathbf{M} = \sum_{\alpha=1}^N \frac{\boldsymbol{\xi}_\alpha \boldsymbol{\xi}_\alpha^\top}{(\mathbf{u}, V_0[\boldsymbol{\xi}_\alpha]\mathbf{u})}, \quad \mathbf{L} = \sum_{\alpha=1}^N \frac{(\mathbf{u}, \boldsymbol{\xi}_\alpha)^2 V_0[\boldsymbol{\xi}_\alpha]}{(\mathbf{u}, V_0[\boldsymbol{\xi}_\alpha]\mathbf{u})^2}. \quad (21)$$

The FNS solves

$$\mathbf{X}\mathbf{u} = \mathbf{0}. \quad (22)$$

by the following iterations [3, 13]:

1. Initialize \mathbf{u} .
2. Compute the matrix \mathbf{X} in (20).
3. Solve the eigenvalue problem

$$\mathbf{X}\mathbf{u}' = \lambda\mathbf{u}', \quad (23)$$

and compute the unit eigenvector \mathbf{u}' for the smallest eigenvalue λ .

4. If $\mathbf{u}' \approx \mathbf{u}$ up to sign, return \mathbf{u}' and stop. Else, let $\mathbf{u} \leftarrow \mathbf{u}'$ and go back to Step 2.

Originally, the eigenvalue closest to 0 was chosen [3] in Step 3. Later, Chojnacki, et al. [5] pointed out that the choice of the smallest eigenvalue improves the convergence. This was also confirmed by the experiments of Kanatani and Sugaya [13]. Whichever eigenvalue is chosen as λ , we have $\lambda = 0$ after convergence. In fact, convergence means

$$\mathbf{X}\mathbf{u} = \lambda\mathbf{u} \quad (24)$$

for some \mathbf{u} . Computing the inner product with \mathbf{u} on both sides, we have

$$(\mathbf{u}, \mathbf{X}\mathbf{u}) = \lambda, \quad (25)$$

but from (20) and (21) we have the identity $(\mathbf{u}, \mathbf{X}\mathbf{u}) = 0$ in \mathbf{u} . Hence, $\lambda = 0$, and \mathbf{u} is the desired solution¹⁰.

HEIV. We can rewrite (22) as

$$\mathbf{M}\mathbf{u} = \mathbf{L}\mathbf{u}. \quad (26)$$

We introduce a new 8-D parameter vector \mathbf{v} , 8-D data vectors \mathbf{z}_α , and their 8×8 normalized covariance matrices $V_0[\mathbf{z}_\alpha]$ in the form

$$\begin{aligned} \boldsymbol{\xi}_\alpha &= \begin{pmatrix} \mathbf{z}_\alpha \\ f_0^2 \end{pmatrix}, & \mathbf{u} &= \begin{pmatrix} \mathbf{v} \\ F_{33} \end{pmatrix}, \\ V_0[\boldsymbol{\xi}_\alpha] &= \begin{pmatrix} V_0[\mathbf{z}_\alpha] & \mathbf{0} \\ \mathbf{0}^\top & 0 \end{pmatrix}. \end{aligned} \quad (27)$$

We define 8×8 matrices

$$\tilde{\mathbf{M}} = \sum_{\alpha=1}^N \frac{\tilde{\mathbf{z}}_\alpha \tilde{\mathbf{z}}_\alpha^\top}{(\mathbf{v}, V_0[\mathbf{z}_\alpha]\mathbf{v})}, \quad \tilde{\mathbf{L}} = \sum_{\alpha=1}^N \frac{(\mathbf{v}, \tilde{\mathbf{z}}_\alpha)^2 V_0[\mathbf{z}_\alpha]}{(\mathbf{v}, V_0[\mathbf{z}_\alpha]\mathbf{v})^2}, \quad (28)$$

where we put

$$\begin{aligned} \tilde{\mathbf{z}}_\alpha &= \mathbf{z}_\alpha - \bar{\mathbf{z}}, \\ \bar{\mathbf{z}} &= \sum_{\alpha=1}^N \frac{\mathbf{z}_\alpha}{(\mathbf{v}, V_0[\mathbf{z}_\alpha]\mathbf{v})} \bigg/ \sum_{\beta=1}^N \frac{1}{(\mathbf{v}, V_0[\mathbf{z}_\beta]\mathbf{v})}. \end{aligned} \quad (29)$$

Then, (26) splits into the following two equations [5, 16]:

$$\tilde{\mathbf{M}}\mathbf{v} = \tilde{\mathbf{L}}\mathbf{v}, \quad (\mathbf{v}, \bar{\mathbf{z}}) + f_0^2 F_{33} = 0. \quad (30)$$

Hence, if an 8-D vector \mathbf{v} that satisfies the first equation is computed, the second equation gives F_{33} , and we obtain

$$\mathbf{u} = N \left[\begin{pmatrix} \mathbf{v} \\ F_{33} \end{pmatrix} \right]. \quad (31)$$

The *HEIV* (*Heteroscedastic Errors-in-Variable*) of Leedan and Meer [16] computes the vector \mathbf{v} that satisfies the first equation in (30) by the following iterations [5, 16]:

¹⁰This crucial fact is inherited to our EFNS to be proposed in Section 5 and plays an essential role for its justification.

1. Initialize \mathbf{v} .
2. Compute the matrices $\tilde{\mathbf{M}}$ and $\tilde{\mathbf{L}}$ in (28).
3. Solve the generalized eigenvalue problem

$$\tilde{\mathbf{M}}\mathbf{v}' = \lambda\tilde{\mathbf{L}}\mathbf{v}', \quad (32)$$

and compute the unit generalized eigenvector \mathbf{v}' for the smallest generalized eigenvalue λ .

4. If $\mathbf{v}' \approx \mathbf{v}$ except for sign, return \mathbf{v}' and stop. Else, let $\mathbf{v} \leftarrow \mathbf{v}'$ and go back to Step 2.

In order to reach the solution of (30), it appears natural to choose as the generalized eigenvalue λ in (32) the one closest to 1. However, Leedan and Meer [16] observed that choosing the smallest one improves the convergence performance. This was also confirmed by the experiments of Kanatani and Sugaya [13]. Whichever generalized eigenvalue is chosen as λ , we have $\lambda = 1$ after convergence. In fact, convergence means

$$\tilde{\mathbf{M}}\mathbf{v} = \lambda\tilde{\mathbf{L}}\mathbf{v} \quad (33)$$

for some \mathbf{v} . Computing the inner product of both sides with \mathbf{v} , we have

$$(\mathbf{v}, \tilde{\mathbf{M}}\mathbf{v}) = \lambda(\mathbf{v}, \tilde{\mathbf{L}}\mathbf{v}), \quad (34)$$

but from (28) we have the identity $(\mathbf{v}, \tilde{\mathbf{M}}\mathbf{v}) = (\mathbf{v}, \tilde{\mathbf{L}}\mathbf{v})$ in \mathbf{v} . Hence, $\lambda = 1$, and \mathbf{u} is the desired solution.

Projective Gauss-Newton iterations. Since the gradient $\nabla_{\mathbf{u}}J$ is given by (19), we can minimize J by Newton iterations. If we evaluate the Hessian $\nabla_{\mathbf{u}}^2J$, the increment $\Delta\mathbf{u}$ in \mathbf{u} is determined by solving

$$(\nabla_{\mathbf{u}}^2J)\Delta\mathbf{u} = -\nabla_{\mathbf{u}}J. \quad (35)$$

Since J is constant in the direction of \mathbf{u} (see (14)), the Hessian $\nabla_{\mathbf{u}}^2J$ is singular, so (35) has infinitely many solutions. From among them, we choose the one orthogonal to \mathbf{u} , using the Moore-Penrose pseudoinverse and computing

$$\Delta\mathbf{u} = -(\nabla_{\mathbf{u}}^2J)_{\bar{\mathbf{g}}}^{-1}\nabla_{\mathbf{u}}J. \quad (36)$$

Differentiating (19) and introducing Gauss-Newton approximation (i.e., ignoring terms that contain $(\mathbf{u}, \boldsymbol{\xi}_\alpha)$), we see that the Hessian is nothing but the matrix $2\mathbf{M}$ in (21). We enforce \mathbf{M} to have eigenvalue 0 for \mathbf{u} , using the projection matrix

$$\mathbf{P}_{\mathbf{u}} = \mathbf{I} - \mathbf{u}\mathbf{u}^\top \quad (37)$$

onto the direction orthogonal to \mathbf{u} . The iteration procedure goes as follows:

1. Initialize \mathbf{u} .
2. Compute

$$\mathbf{u}' = N[\mathbf{u} - (\mathbf{P}_{\mathbf{u}}\mathbf{M}\mathbf{P}_{\mathbf{u}})_{\bar{\mathbf{g}}}^{-1}(\mathbf{M} - \mathbf{L})\mathbf{u}]. \quad (38)$$

3. If $\mathbf{u}' \approx \mathbf{u}$, return \mathbf{u}' and stop. Else, let $\mathbf{u} \leftarrow \mathbf{u}'$ and go back to Step 2.

3.3 Initialization

The FNS, the HEIV, and the projective Gauss-Newton are all iterative method, so they require initial values. The best known non-iterative procedures are the least squares and the Taubin method.

Least squares (LS). This is the most popular method, also known as the *algebraic distance minimization* or the *8-point algorithm* [6]. Approximating the denominators in (14) by a constant, we minimize

$$J_{\text{LS}} = \sum_{\alpha=1}^N (\mathbf{u}, \boldsymbol{\xi}_{\alpha})^2 = (\mathbf{u}, \mathbf{M}_{\text{LS}}\mathbf{u}), \quad (39)$$

where we define

$$\mathbf{M}_{\text{LS}} = \sum_{\alpha=1}^N \boldsymbol{\xi}_{\alpha} \boldsymbol{\xi}_{\alpha}^{\top}. \quad (40)$$

The function J_{LS} can be minimized by the unit eigenvector of \mathbf{M}_{LS} for the smallest eigenvalue.

Taubin method. Replacing the denominators in (14) by their average, we minimize the following function¹¹ [26]:

$$J_{\text{TB}} = \frac{\sum_{\alpha=1}^N (\mathbf{u}, \boldsymbol{\xi}_{\alpha})^2}{\sum_{\alpha=1}^N (\mathbf{u}, V_0[\boldsymbol{\xi}_{\alpha}]\mathbf{u})} = \frac{(\mathbf{u}, \mathbf{M}_{\text{LS}}\mathbf{u})}{(\mathbf{u}, \mathbf{N}_{\text{TB}}\mathbf{u})}. \quad (41)$$

The matrix \mathbf{N}_{TB} has the form

$$\mathbf{N}_{\text{TB}} = \sum_{\alpha=1}^N V_0[\boldsymbol{\xi}_{\alpha}]. \quad (42)$$

The function J_{TB} can be minimized by solving the generalized eigenvalue problem

$$\mathbf{M}_{\text{LS}}\mathbf{u} = \lambda \mathbf{N}_{\text{TB}}\mathbf{u} \quad (43)$$

for the smallest generalized eigenvalue. However, we cannot directly solve this, because \mathbf{N}_{TB} is not positive definite. So, we decompose $\boldsymbol{\xi}_{\alpha}$, \mathbf{u} , and $V_0[\boldsymbol{\xi}_{\alpha}]$ in the form of (27) and define 8×8 matrices $\tilde{\mathbf{M}}_{\text{LS}}$ and $\tilde{\mathbf{N}}_{\text{TB}}$ by

$$\tilde{\mathbf{M}}_{\text{LS}} = \sum_{\alpha=1}^N \tilde{\mathbf{z}}_{\alpha} \tilde{\mathbf{z}}_{\alpha}^{\top}, \quad \tilde{\mathbf{N}}_{\text{LS}} = \sum_{\alpha=1}^N V_0[\mathbf{z}_{\alpha}], \quad (44)$$

where

$$\tilde{\mathbf{z}}_{\alpha} = \mathbf{z}_{\alpha} - \bar{\mathbf{z}}, \quad \bar{\mathbf{z}} = \frac{1}{N} \sum_{\alpha=1}^N \mathbf{z}_{\alpha}. \quad (45)$$

Then, (43) splits into two equations

$$\tilde{\mathbf{M}}_{\text{LS}}\mathbf{v} = \lambda \tilde{\mathbf{N}}_{\text{TB}}\mathbf{v}, \quad (\mathbf{v}, \bar{\mathbf{z}}) + f_0^2 F_{33} = 0. \quad (46)$$

¹¹Taubin [26] did not take the covariance matrix into account. This is a modification of his method.

We compute the unit generalized eigenvector \mathbf{v} of the first equation for the smallest generalized eigenvalue λ . The second equation gives F_{33} , and \mathbf{u} is given in the form of (31). It has been shown that the Taubin method produces a very accurate close to the unconstrained ML solution [12, 13].

4. Internal Access

The fundamental matrix \mathbf{F} has nine elements, on which the normalization $\|\mathbf{F}\| = 1$ and the rank constraint $\det \mathbf{u} = 0$ are imposed. Hence, it has seven degrees of freedom. The internal access approach minimizes (14) by searching the reduced 7-D parameter space (Fig. 1(b)).

Many types of 7-degree parameterizations have been obtained, e.g., by algebraic elimination of the rank constraint or by expressing the fundamental matrix in terms of epipoles [22, 28], but the resulting expressions are complicated, and the geometric meaning of the individual unknowns are not clear. This was overcome by Bartoli and Sturm [1], who regarded the SVD of \mathbf{F} as its parameterization. Their expression is compact, and each parameter has its geometric meaning. However, they included, in addition to \mathbf{F} , the tentatively reconstructed 3-D positions of the observed feature points, the relative positions of the two cameras, and their intrinsic parameters as unknowns and minimized the reprojection error; such an approach is known as *bundle adjustment*. Since the tentative 3-D reconstruction from two images is indeterminate, they chose the one for which the first camera matrix is in a particular form (“canonical form”).

Here, we avoid this complication by directly minimizing (14) by the Levenberg-Marquardt (LM) method, using the parameterization of Bartoli and Sturm [1]

$$\mathbf{F} = \mathbf{U} \text{diag}(\sigma_1, \sigma_2, 0) \mathbf{V}^{\top}, \quad (47)$$

where \mathbf{U} and \mathbf{V} are orthogonal matrices, and σ_1 and σ_2 are the singular values. Since the normalization $\|\mathbf{F}\|^2 = 1$ is equivalent to $\sigma_1^2 + \sigma_2^2 = 1$ (see Appendix A), we adopt the following representation¹²:

$$\sigma_1 = \cos \theta, \quad \sigma_2 = \sin \theta. \quad (48)$$

If the principal point is at the origin (0, 0) and if there are no image distortions, θ takes the value $\pi/4$ (i.e., $\sigma_1 = \sigma_2$) [7, 10].

The orthogonal matrices \mathbf{U} and \mathbf{V} have three degrees of freedom each, so they and θ constitute the seven degrees of freedom. However, the analysis becomes complicated if \mathbf{U} and \mathbf{V} are directly expressed in three parameters each (e.g., the Euler angles or the rotations around each coordinate axis). Following Bartoli and Sturm [1], we adopt the “Lie algebraic

¹²Bartoli and Sturm [1] took the ratio $\gamma = \sigma_2/\sigma_1$ as a variable. Here, we adopt the angle θ for the symmetry.

method" [9]: we represent the "increment" in \mathbf{U} and \mathbf{V} by three parameters each. Let ω_1, ω_2 , and ω_3 represent the increment in \mathbf{U} , and ω'_1, ω'_2 , and ω'_3 in \mathbf{V} . The derivatives of (14) with respect to them are as follows (see Appendix A):

$$\nabla_{\omega} J = 2\mathbf{F}_U^{\top} \mathbf{X} \mathbf{u}, \quad \nabla_{\omega'} J = 2\mathbf{F}_V^{\top} \mathbf{X} \mathbf{u}. \quad (49)$$

Here, \mathbf{X} is the matrix in (20), and \mathbf{F}_U , and \mathbf{F}_V are defined by

$$\mathbf{F}_U = \begin{pmatrix} 0 & F_{31} & -F_{21} \\ 0 & F_{32} & -F_{22} \\ 0 & F_{33} & -F_{23} \\ -F_{31} & 0 & F_{11} \\ -F_{32} & 0 & F_{12} \\ -F_{33} & 0 & F_{13} \\ F_{21} & -F_{11} & 0 \\ F_{22} & -F_{12} & 0 \\ F_{23} & -F_{13} & 0 \end{pmatrix}, \quad \mathbf{F}_V = \begin{pmatrix} 0 & F_{13} & -F_{12} \\ -F_{13} & 0 & F_{11} \\ F_{12} & -F_{11} & 0 \\ 0 & F_{23} & -F_{22} \\ -F_{23} & 0 & F_{21} \\ F_{22} & -F_{21} & 0 \\ 0 & F_{33} & -F_{32} \\ -F_{33} & 0 & F_{31} \\ F_{32} & -F_{31} & 0 \end{pmatrix}. \quad (50)$$

The derivative of (14) with respect to θ has the form (see Appendix A)

$$\frac{\partial J}{\partial \theta} = (\mathbf{u}_{\theta}, \mathbf{X} \mathbf{u}), \quad (51)$$

where we define

$$\mathbf{u}_{\theta} = \begin{pmatrix} U_{12}V_{12} \cos \theta - U_{11}V_{11} \sin \theta \\ U_{12}V_{22} \cos \theta - U_{11}V_{21} \sin \theta \\ U_{12}V_{32} \cos \theta - U_{11}V_{31} \sin \theta \\ U_{22}V_{12} \cos \theta - U_{21}V_{11} \sin \theta \\ U_{22}V_{22} \cos \theta - U_{21}V_{21} \sin \theta \\ U_{22}V_{32} \cos \theta - U_{21}V_{31} \sin \theta \\ U_{32}V_{12} \cos \theta - U_{31}V_{11} \sin \theta \\ U_{32}V_{22} \cos \theta - U_{31}V_{21} \sin \theta \\ U_{32}V_{32} \cos \theta - U_{31}V_{31} \sin \theta \end{pmatrix}. \quad (52)$$

Adopting Gauss-Newton approximation, which amounts to ignoring terms involving $(\mathbf{u}, \boldsymbol{\xi}_{\alpha})$, we obtain the second derivatives as follows (see Appendix A):

$$\begin{aligned} \nabla_{\omega}^2 J &= 2\mathbf{F}_U^{\top} \mathbf{M} \mathbf{F}_U, & \nabla_{\omega'}^2 J &= 2\mathbf{F}_V^{\top} \mathbf{M} \mathbf{F}_V, \\ \nabla_{\omega \omega'} J &= 2\mathbf{F}_U^{\top} \mathbf{M} \mathbf{F}_V, & \frac{\partial J^2}{\partial \theta^2} &= 2(\mathbf{u}_{\theta}, \mathbf{M} \mathbf{u}_{\theta}), \\ \frac{\partial \nabla_{\omega} J}{\partial \theta} &= 2\mathbf{F}_U^{\top} \mathbf{M} \mathbf{u}_{\theta}, & \frac{\partial \nabla_{\omega'} J}{\partial \theta} &= 2\mathbf{F}_V^{\top} \mathbf{M} \mathbf{u}_{\theta}. \end{aligned} \quad (53)$$

The 7-parameter LM search goes as follows:

1. Initialize $\mathbf{F} = \mathbf{U} \text{diag}(\cos \theta, \sin \theta, 0) \mathbf{V}^{\top}$.
2. Compute J in (14), and let $c = 0.0001$.
3. Compute \mathbf{F}_U , \mathbf{F}_V , and \mathbf{u}_{θ} in (50) and (52).
4. Compute \mathbf{X} in (20), the first derivatives in (49) an (51), and the second derivatives in (53).
5. Compute the following matrix \mathbf{H} :

$$\mathbf{H} = \begin{pmatrix} \nabla_{\omega}^2 J & \nabla_{\omega \omega'} J & \partial \nabla_{\omega} J / \partial \theta \\ (\nabla_{\omega \omega'} J)^{\top} & \nabla_{\omega'}^2 J & \partial \nabla_{\omega'} J / \partial \theta \\ (\partial \nabla_{\omega} J / \partial \theta)^{\top} & (\partial \nabla_{\omega'} J / \partial \theta)^{\top} & \partial J^2 / \partial \theta^2 \end{pmatrix}. \quad (54)$$

6. Solve the 7-D simultaneous linear equations

$$(\mathbf{H} + cD[\mathbf{H}]) \begin{pmatrix} \boldsymbol{\omega} \\ \boldsymbol{\omega}' \\ \Delta \theta \end{pmatrix} = - \begin{pmatrix} \nabla_{\omega} J \\ \nabla_{\omega'} J \\ \partial J / \partial \theta \end{pmatrix}, \quad (55)$$

for $\boldsymbol{\omega}$, $\boldsymbol{\omega}'$, and $\Delta \theta$, where $D[\cdot]$ denotes the diagonal matrix obtained by taking out only the diagonal elements.

7. Update \mathbf{U} , \mathbf{V} , and θ by

$$\mathbf{U}' = \mathcal{R}(\boldsymbol{\omega}) \mathbf{U}, \quad \mathbf{V}' = \mathcal{R}(\boldsymbol{\omega}') \mathbf{V}, \quad \theta' = \theta + \Delta \theta, \quad (56)$$

where $\mathcal{R}(\boldsymbol{\omega})$ denotes rotation around $N[\boldsymbol{\omega}]$ by angle $\|\boldsymbol{\omega}\|$.

8. Update \mathbf{F} as follows:

$$\mathbf{F}' = \mathbf{U}' \text{diag}(\cos \theta', \sin \theta', 0) \mathbf{V}'^{\top}. \quad (57)$$

9. Let J' be the value of (14) for \mathbf{F}' .
10. Unless $J' < J$ or $J' \approx J$, let $c \leftarrow 10c$, and go back to Step 6.
11. If $\mathbf{F}' \approx \mathbf{F}$, return \mathbf{F}' and stop. Else, let $\mathbf{F} \leftarrow \mathbf{F}'$, $\mathbf{U} \leftarrow \mathbf{U}'$, $\mathbf{V} \leftarrow \mathbf{V}'$, $\theta \leftarrow \theta'$, and $c \leftarrow c/10$, and go back to Step 3.

5. External Access

The external access approach does iterations in the 9-D \mathbf{u} -space in such a way that an optimal solution satisfying the rank constraint automatically results (Fig. 1(c)). The concept dates back to such heuristics as introducing penalties to the violation of the constraints or projecting the solution onto the surface of the constraints in the course of iterations, but it is Chojnacki et al. [4] that first presented a systematic scheme called CFNS.

Stationarity Condition. According to the variational principle, the necessary and sufficient condition for the function J to be stationary at a point \mathbf{u} in \mathcal{S}^8 in \mathcal{R}^9 is that its gradient $\nabla_{\mathbf{u}} J$ is orthogonal to the hypersurface defined by $\det \mathbf{u} = 0$ (or equivalently by (10)); its surface normal is given by the cofactor vector \mathbf{u}^{\dagger} , which is orthogonal to \mathbf{u} (see (10)). However, $\nabla_{\mathbf{u}} J = \mathbf{X} \mathbf{u}$ is always tangent to \mathcal{S}^8 , because of the identity $(\mathbf{u}, \nabla_{\mathbf{u}} J) = (\mathbf{u}, \mathbf{X} \mathbf{u}) = 0$ in \mathbf{u} . So, $\nabla_{\mathbf{u}} J$

should be parallel to the cofactor vector \mathbf{u}^\dagger . This means that if we define the projection matrix

$$\mathbf{P}_{\mathbf{u}^\dagger} = \mathbf{I} - \mathbf{u}^\dagger \mathbf{u}^{\dagger\top} \quad (58)$$

onto the direction orthogonal to the cofactor vector \mathbf{u}^\dagger , the stationarity condition is written as

$$\mathbf{P}_{\mathbf{u}^\dagger} \mathbf{X} \mathbf{u} = \mathbf{0}. \quad (59)$$

The rank constraint of (10) is written as $\mathbf{P}_{\mathbf{u}^\dagger} \mathbf{u} = \mathbf{u}$. Combined with (59), the desired solution should be such that

$$\mathbf{Y} \mathbf{u} = \mathbf{0}, \quad \mathbf{P}_{\mathbf{u}^\dagger} \mathbf{u} = \mathbf{u}, \quad (60)$$

where we define

$$\mathbf{Y} = \mathbf{P}_{\mathbf{u}^\dagger} \mathbf{X} \mathbf{P}_{\mathbf{u}^\dagger}. \quad (61)$$

CFNS. Chojnacki et al. [4] showed that the stationarity condition of (60) is written as a single equation in the form

$$\mathbf{Q} \mathbf{u} = \mathbf{0}, \quad (62)$$

where \mathbf{Q} is a rather complicated symmetric matrix (see Appendix B). They proposed to solve (62) by iterations in the same form as their FNS and called it *CFNS* (*Constrained FNS*):

1. Initialize \mathbf{u} .
2. Compute the matrix \mathbf{Q} .
3. Solve the eigenvalue problem

$$\mathbf{Q} \mathbf{u}' = \lambda \mathbf{u}', \quad (63)$$

and compute the unit eigenvector \mathbf{u}' for the eigenvalue λ closest to 0.

4. If $\mathbf{u}' \approx \mathbf{u}$ up to sign, return \mathbf{u}' and stop. Else, let $\mathbf{u} \leftarrow \mathbf{u}'$, and go back to Step 2.

Infinitely many candidates exist for the matrix \mathbf{Q} with which the problem is written as (62), but not all of them allow the above iterations to converge. Chojnacki et al. [4] gave the one shown in Appendix B, but the derivation is not written in their paper. We later show that CFNS does not necessarily converge to a correct solution.

EFNS. We now present a new iterative scheme, which we call *EFNS* (*Extended FNS*), for solving (60). The procedure goes as follows:

1. Initialize \mathbf{u} .
2. Compute the matrix \mathbf{X} in (20), the projection matrix $\mathbf{P}_{\mathbf{u}^\dagger}$ in (58), and the matrix \mathbf{Y} in (61).
3. Solve the eigenvalue problem

$$\mathbf{Y} \mathbf{v} = \lambda \mathbf{v}, \quad (64)$$

and compute the two unit eigenvectors \mathbf{v}_1 and \mathbf{v}_2 for the smallest eigenvalues in absolute terms.

4. Compute the following vector $\hat{\mathbf{u}}$:

$$\hat{\mathbf{u}} = (\mathbf{u}, \mathbf{v}_1) \mathbf{v}_1 + (\mathbf{u}, \mathbf{v}_2) \mathbf{v}_2. \quad (65)$$

5. Compute

$$\mathbf{u}' = N[\mathbf{P}_{\mathbf{u}^\dagger} \hat{\mathbf{u}}]. \quad (66)$$

6. If $\mathbf{u}' \approx \mathbf{u}$, return \mathbf{u}' and stop. Else, let $\mathbf{u} \leftarrow N[\mathbf{u} + \mathbf{u}']$ and go back to Step 2.

Justification. We first show that when the above iterations have converged, the eigenvectors \mathbf{v}_1 and \mathbf{v}_2 both have eigenvalue 0. From the definition of \mathbf{Y} in (61) and $\mathbf{P}_{\mathbf{u}^\dagger}$ in (58), the cofactor vector \mathbf{u}^\dagger is always an eigenvector of \mathbf{Y} with eigenvalue 0. This means that either \mathbf{v}_1 or \mathbf{v}_2 has eigenvalue 0. Suppose one, say \mathbf{v}_1 , has nonzero eigenvalue λ ($\neq 0$). Then, $\mathbf{v}_2 = \pm \mathbf{u}^\dagger$.

By construction, the vector $\hat{\mathbf{u}}$ in (65) belongs to the linear span of \mathbf{v}_1 and \mathbf{v}_2 ($= \pm \mathbf{u}^\dagger$), which are mutually orthogonal, and the vector \mathbf{u}' in (66) is a projection of $\hat{\mathbf{u}}$ within that linear span onto the direction orthogonal to the cofactor vector \mathbf{u}^\dagger . Hence, it coincides with $\pm \mathbf{v}_1$. After the iterations have converged, we have $\mathbf{u} = \mathbf{u}'$ ($= \pm \mathbf{v}_1$), so \mathbf{v}_1 is an eigenvector of \mathbf{Y} with eigenvalue λ . Hence, \mathbf{u} also satisfies (64). Computing the inner product with \mathbf{u} on both sides, we have

$$(\mathbf{u}, \mathbf{Y} \mathbf{u}) = \lambda. \quad (67)$$

On the other hand, \mathbf{u} ($= \pm \mathbf{v}_1$) is orthogonal to the cofactor vector \mathbf{u}^\dagger ($= \pm \mathbf{v}_2$), so

$$\mathbf{P}_{\mathbf{u}^\dagger} \mathbf{u} = \mathbf{u}. \quad (68)$$

Hence,

$$(\mathbf{u}, \mathbf{Y} \mathbf{u}) = (\mathbf{u}, \mathbf{P}_{\mathbf{u}^\dagger} \mathbf{X} \mathbf{P}_{\mathbf{u}^\dagger} \mathbf{u}) = (\mathbf{u}, \mathbf{X} \mathbf{u}) = 0, \quad (69)$$

since $(\mathbf{u}, \mathbf{X} \mathbf{u}) = 0$ is an identity in \mathbf{u} (see (20) and also (21) and footnote 10). However, (67) and (69) contradict our assumption that $\lambda \neq 0$. So, \mathbf{v}_1 is also an eigenvector of \mathbf{Y} with eigenvalue 0. \square

It follows that the two equations in (60) hold, and hence \mathbf{u} is the desired solution. Of course, this conclusion relies on the premise that the iterations converge. According to our experience, if we let $\mathbf{u} \leftarrow \mathbf{u}'$ in Step 9, the next value of \mathbf{u}' computed in Step 8 often reverts to the former value of \mathbf{u} , falling in infinite looping. So, we update \mathbf{u} to the ‘‘midpoint’’ $(\mathbf{u}' + \mathbf{u})/2$ and normalized it to a unit vector $N[\mathbf{u}' + \mathbf{u}]$ in Step 9. The convergence performance is greatly improved by this. In fact, we have observed that this same technique can also improve the convergence performance of the ordinary FNS, which sometimes oscillates in the presence of very large noise.

CFNS vs. EFNS. Fig. 3 shows simulated images of two planar grid surfaces viewed from different angles.

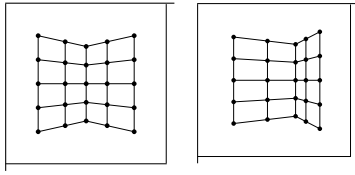


Figure 3: Simulated images of planar grid surfaces.

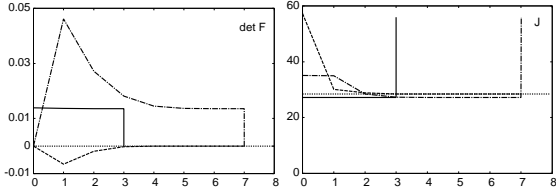


Figure 4: The convergence of $\det \mathbf{F}$ and the residual J for different initializations ($\sigma = 1$): LS (solid line), SVD-corrected LS (dashed line), and the true value (chained line). All solutions are SVD-corrected in the final step.

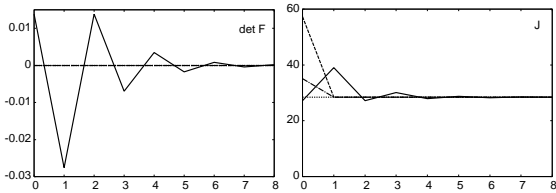


Figure 5: The results by EFNS corresponding to Fig. 5.

The image size is 600×600 pixels with 1200 pixel focal length. We added random Gaussian noise of mean 0 and standard deviation σ to the x - and y -coordinates of each grid point independently and from them computed the fundamental matrix by CFNS and EFNS.

Fig. 4 shows a typical instance ($\sigma = 1$) of the convergence of the determinant $\det \mathbf{F}$ and the residual J from different initial values. In the final step, $\det \mathbf{F}$ is forced to be 0 by SVD, as prescribed by Chojnacki et al. [4]. The dotted lines show the values to be converged.

The LS solution has a very low residual J , since the rank constraint $\det \mathbf{F} = 0$ is ignored. So, J needs to be increased to achieve $\det \mathbf{F} = 0$, but CFNS fails to do so. As a result, $\det \mathbf{F}$ remains nonzero and drops to 0 by the final SVD correction, causing a sudden jump in J . If we start from SVD-corrected LS, the residual J first increases, making $\det \mathbf{F}$ nonzero, but in the end both J and $\det \mathbf{F}$ converge in an expected way. In contrast, the true value has a very large J , so CFNS tries to decrease it sharply at the cost of too much increase in $\det \mathbf{F}$, which never reverts to 0 until the final SVD. Fig. 5 shows corresponding results by EFNS. Both J and $\det \mathbf{F}$ converge to their correct values with stably attenuating oscillations. Figs. 6

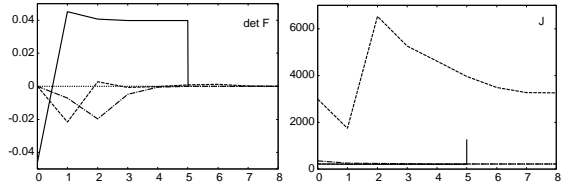


Figure 6: The convergence of $\det \mathbf{F}$ and the residual J for different initializations ($\sigma = 3$): LS (solid line), SVD-corrected LS (dashed line), and the true value (chained line). All solutions are SVD-corrected in the final step.

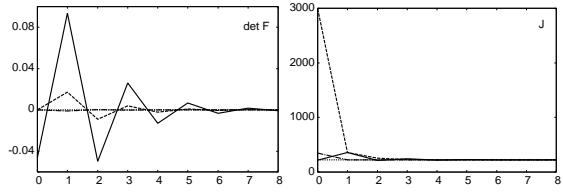


Figure 7: The results by EFNS corresponding to Fig. 6.

and 7 show the results corresponding to Fig. 4 and 5 for another instance ($\sigma = 3$). We can observe similar behavior of CFNS and EFNS.

We mean by “convergence” the state of the same solution repeating itself in the course of iterations. In mathematical terms, the resulting solution is a *fixed point* of the iteration operator, i.e., the procedure to update the current solution. In [4], Chojnacki et al. [4] proved that the solution \mathbf{u} satisfying (60) is a fixed point of their CFNS. Apparently, they expected to arrive at that solution by their scheme. As demonstrated by Figs. 4, and 6, however, CFNS has many other fixed points, and which to arrive at depends on initialization. In contrast, we have proved that any fixed point of EFNS is *necessarily* the desired solution.

6. Accuracy Comparison

Using the simulated images in Fig. 3, we compare the accuracy of the following methods:

- 1) SVD-corrected LS (Hartley’s 8-point method)
- 2) SVD-corrected ML
- 3) CFNS of Chojnacki et al.
- 4) Optimally corrected ML
- 5) 7-parameter LM
- 6) EFNS

For brevity, we use the shorthand “ML” for unconstrained minimization of (14), for which we used the FNS of Chojnacki et al. [3] initialized by LS. We confirmed that FNS, HEIV, and the projective Gauss-Newton iterations all converged to the same solution (up to rounding errors), although the speed of convergence varies (see [13] for the convergence comparison).

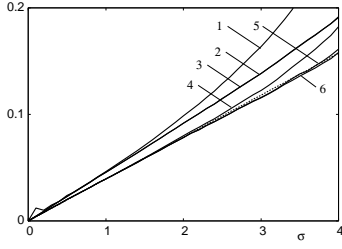


Figure 8: The RMS error D vs. noise level σ for Fig. 3. 1) SVD-corrected LS. 2) SVD-corrected ML. 3) CFNS. 4) Optimally corrected ML. 5) 7-parameter LM. 6) EFNS. The dotted line indicates the KCR lower bound.

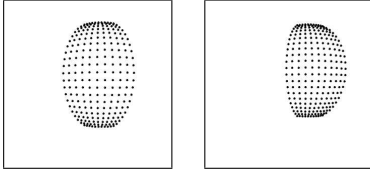


Figure 9: Simulated images of a spherical grid surface.

We initialized the 7-parameter LM, CFNS, and EFNS by LS. All iterations are stopped when the update of \mathbf{F} is less than 10^{-6} in norm.

Fig. 8 plots for the noise level σ on the horizontal axis the following root-mean-square (RMS) error D corresponding to (8) over 10000 independent trials:

$$D = \sqrt{\frac{1}{10000} \sum_{a=1}^{10000} \|\mathbf{P}_U \hat{\mathbf{u}}^{(a)}\|^2}. \quad (70)$$

Here, $\hat{\mathbf{u}}^{(a)}$ is the a th value, and \mathbf{P}_U is the projection matrix in (11); since the solution is normalized into a unit vector, we measure the deviation of $\hat{\mathbf{u}}^{(a)}$ from \mathbf{u} by orthogonally projecting $\hat{\mathbf{u}}^{(a)}$ onto the tangent space $T_{\mathbf{u}}(\mathcal{U})$ to \mathcal{U} at \mathbf{u} (see (8) and Fig. 2). The dotted line is the value implied by the KCR lower bound (the trace of the right-hand side of (12)).

Note that the RMS error D describes not the simple “average” of the error but its “variation” from zero; the computed solution is often very close to the true value but sometimes very far from it, and D measures the “standard deviation” of the scatter.

Fig. 9 shows simulated images (600×600 pixels) of a spherical grid surface viewed from different angles. We did similar experiments, and Fig. 10 shows the results corresponding to Fig. 8.

Preliminary observations. We can see that SVD-corrected LS (Hartley’s 8-point algorithm) performs very poorly. We can also see that SVD-corrected ML is inferior to optimally corrected ML, whose accuracy is close to the KCR lower bound. The accuracy of the 7-parameter LM is nearly the same as optimally corrected ML when the noise is small but gradually outperforms it as the noise increases. Best performing is EFNS, exhibiting nearly the same accuracy as

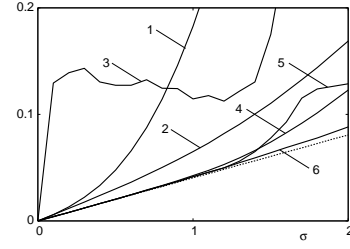


Figure 10: The RMS error D vs. noise level σ for Fig. 9. 1) SVD-corrected LS. 2) SVD-corrected ML. 3) CFNS. 4) Optimally corrected ML. 5) 7-parameter LM. 6) EFNS. The dotted line indicates the KCR lower bound.

the KCR lower bound. The CFNS performs as poorly as SVD-corrected ML, because, as we observed in the preceding section, it is likely to stop at the unconstrained ML solution (we forced the determinant to be zero by SVD). Doing many experiments (not all shown here), we have observed that:

- i) The EFNS stably achieves the highest accuracy over a wide range of the noise level.
- ii) Optimally corrected ML is fairly accurate and very robust to noise but gradually deteriorates as noise grows.
- iii) The 7-parameter LM achieves very high accuracy when started from a good initial value but is likely to fall into local minima if poorly initialized.

The robustness of EFNS and optimally corrected ML is due to the fact that the computation is done in the redundant (“external”) \mathbf{u} -space, where J has a simple form of (14). In fact, we have never experienced local minima in our experiments. The deterioration of optimally corrected ML in the presence of large noise is because linear approximation is involved in (17).

The fragility of the 7-parameter LM is attributed to the complexity of the function J when expressed in seven parameters, resulting in many local minima in the reduced (“internal”) parameter space, as pointed out in [22].

Thus, the optimal correction of ML and the 7-parameter ML have complementary characteristics, which suggests that the 7-parameter ML started from optimally corrected ML may exhibit comparable accuracy to EFNS. We now confirm this.

Detailed observations. Fig. 11 compares for the images in Fig. 3:

- 1) optimally corrected ML.
- 2) 7-parameter LM started from LS.
- 3) 7-parameter LM started from optimally corrected ML.
- 4) EFNS.

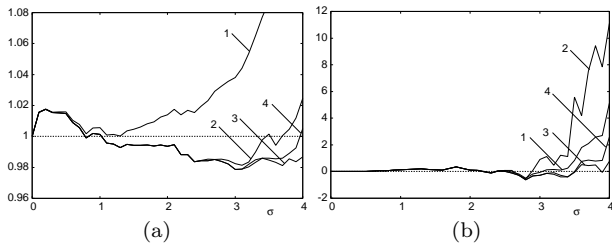


Figure 11: (a) The RMS error relative to the KCR lower bound and (b) the average residual minus minus $(N-7)\sigma^2$ for Fig. 3. 1) Optimally corrected ML. 2) 7-parameter LM started from LS. 3) 7-parameter LM started from optimally corrected ML. 4) EFNS.

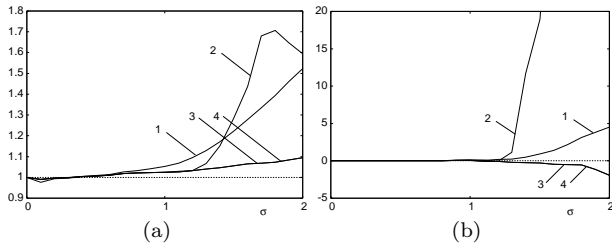


Figure 12: (a) The RMS error relative to the KCR lower bound and (b) the average residual minus minus $(N-7)\sigma^2$ for Fig. 9. 1) Optimally corrected ML. 2) 7-parameter LM started from LS. 3) 7-parameter LM started from optimally corrected ML. 4) EFNS.

For visual ease, we plot in Fig. 11(a) the ratio D/D_{KCR} of D in (70) to the corresponding KCR lower bound. Fig. 11(b) plots the average residual \hat{J} (minimum of (14)). Since direct plots of \hat{J} nearly overlap for all the methods, we display here the difference $\hat{J} - (N-7)\sigma^2$, where N is the number of corresponding pairs. This is motivated by the fact that to a first approximation \hat{J}/σ^2 is subject to a χ^2 distribution with $N-7$ degrees of freedom [10], so the expectation of \hat{J} is approximately $(N-7)\sigma^2$. Fig. 12 shows the corresponding results for Fig. 9. We observe:

- i) The RMS error of optimally corrected ML increases as noise increases, *yet* the corresponding residual remains low.
- ii) The 7-parameter LM started from LS appears to have small RMS errors for noise levels for which the corresponding residual is *high*, though.
- iii) The accuracy of the 7-parameter LM improves if started from optimally corrected ML, resulting in the accuracy comparable to EFNS.

The seeming contradiction that solutions that are closer to the true value (measured in the RMS error) have higher residuals \hat{J} implies that the LM search failed to reach the true minimum of J , indicating existence of local minima located closer to the true value than to the true minimum of J . When started

from optimally corrected ML, the LM search successfully reaches the true minimum of J , resulting in the smaller \hat{J} but *larger* RMS errors.

RMS vs. KCR Lower Bound. One may wonder why the computed RMS errors are sometimes below the KCR lower bound. There are several reasons for this.

The KCR lower bound is shown here for a convenient reference, but it does not mean that errors of the values computed by any *algorithm* should be above it; it is a lower bound on *unbiased estimators*. By “estimator”, we mean a *function* of the data, e.g., the minimizer of a given cost function. An iterative algorithm such as LM does not qualify as an estimator, since the final value depends not only on the data but also on the starting value; the resulting value may not be the true minimizer of the cost function. Thus, it may happen, as we have observed, that a solution closer to the true value has higher residual.

Next, the KCR lower bound is derived, without any approximation [10], from the starting identity that the expectation of the estimator (as a “function” of the data) should coincide with its true value. This is a very strong identity, from which the KCR lower bound is derived using integral transformations in the same way as the Cramer-Rao lower bound is from the unbiasedness constraint in the framework of traditional statistical estimation. However, the ML estimator or the minimizer of the function J in (14) may not necessarily be unbiased when the noise is large. In fact, it has been reported that removing bias from the ML solution can result in better accuracy (“hyperaccuracy”) for ellipse fitting in the presence of large noise [12, 11].

Finally, the RMS error is computed from “finite” samples, while the KCR lower bound is a theoretical “expectation”. We did 10000 independent trials for each σ , but the result still has fluctuations. Theoretically, the plot should be a smooth function of σ , but zigzags remain to some extent how many samples we use.

Which is better? We have seen the best performance exhibited by the 7-parameter ML started from optimally corrected ML and by EFNS. Now, we test which is really better, using a hybrid method: we try both methods and choose the solution that has a smaller residual \hat{J} . Fig. 13 plots the ratio of each solution being chosen for the images in Figs. 3 and 9. As we can see, the two methods are completely even with no preference of one to the other.

7. Bundle Adjustment

There is a subtle point to be clarified in the discussion of Section 2. The transition from (13) to (14) is exact; no approximation is involved. Although terms of $O(\sigma^4)$ are omitted and the true values are replaced

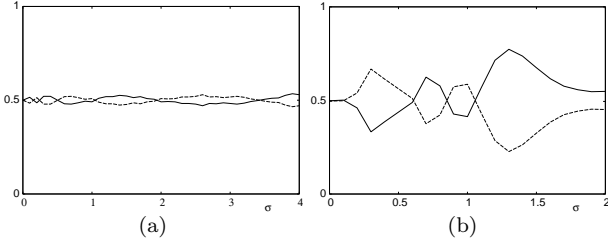


Figure 13: The ratio of the solution being chosen for (a) Fig. 3 and (b) for Fig. 9. Solid line: 7-parameter LM started from optimally corrected ML. Dashed line: EFNS.

by their data in (7), it is numerically confirmed that the final results are not affected in any noticeable way. This is also justified by a simple order analysis: because the numerator on the right-hand side of (14) is $O(\sigma^2)$, while the denominator is $O(1)$, any small perturbation in the denominator causes only a higher order perturbation of J .

However, although the “analysis” may be correct, the “interpretation” is not strict. Namely, despite the fact that (14) is the (squared) Mahalanobis distance in the ξ -space, its minimization can be ML only when the noise in the ξ -space is Gaussian, because then and only then is the likelihood proportional to $e^{-J/\text{constant}}$. Strictly speaking, if the noise in the image plane is Gaussian, the transformed noise in the ξ -space is no longer Gaussian, so the proviso that “If the noise in $\{\xi_\alpha\}$ is ...” above (13) (and for the KCR lower bound of (12), too) does not necessarily hold, and minimizing (14) is not strictly ML in the image plane.

In order to test how much difference is incurred by this, we minimize the Mahalanobis distance in the $\{\mathbf{x}, \mathbf{x}'\}$ -space, called the *reprojection error*. This approach was endorsed by Hartley and Zisserman [7], who called it the *Gold Standard*. So far, however, no simple procedure existed for minimizing the reprojection error subject to the epipolar equation with a rank-constrained fundamental matrix. So, this problem has usually been done as search in an “augmented” parameter space, as done by Bartoli and Sturm [1], computing tentative 3-D reconstruction and adjusting the reconstructed shape, the camera positions, and the intrinsic parameters so that the resulting projection images are as close to the input images as possible. Such a strategy is called *bundle adjustment*.

Here, we present a new numerical scheme for directly minimizing the reprojection error without reference to any tentative 3-D reconstruction; the computation is done *solely in the domain of the fundamental matrix* \mathbf{F} . We compare its accuracy with those methods we described so far.

Problem. We minimize the reprojection error

$$E = \sum_{\alpha=1}^N \left(\|\mathbf{x}_\alpha - \bar{\mathbf{x}}_\alpha\|^2 + \|\mathbf{x}'_\alpha - \bar{\mathbf{x}}'_\alpha\|^2 \right), \quad (71)$$

with respect to $\bar{\mathbf{x}}_\alpha$, $\bar{\mathbf{x}}'_\alpha$, $\alpha = 1, \dots, N$, and \mathbf{F} (constrained to be $\|\mathbf{F}\| = 1$ and $\det \mathbf{F} = 0$) subject to the epipolar equation

$$(\bar{\mathbf{x}}_\alpha, \mathbf{F}\bar{\mathbf{x}}'_\alpha) = 0, \quad \alpha = 1, \dots, N. \quad (72)$$

First approximation. Instead of estimating $\bar{\mathbf{x}}_\alpha$ and $\bar{\mathbf{x}}'_\alpha$ directly, we may alternatively express them as

$$\bar{\mathbf{x}}_\alpha = \mathbf{x}_\alpha - \Delta\mathbf{x}_\alpha, \quad \bar{\mathbf{x}}'_\alpha = \mathbf{x}'_\alpha - \Delta\mathbf{x}'_\alpha, \quad (73)$$

and estimate the correction terms $\Delta\mathbf{x}_\alpha$ and $\Delta\mathbf{x}'_\alpha$. Substituting (73) into (71), we have

$$E = \sum_{\alpha=1}^N \left(\|\Delta\mathbf{x}_\alpha\|^2 + \|\Delta\mathbf{x}'_\alpha\|^2 \right). \quad (74)$$

The epipolar equation of (72) becomes

$$(\mathbf{x}_\alpha - \Delta\mathbf{x}_\alpha, \mathbf{F}(\mathbf{x}'_\alpha - \Delta\mathbf{x}'_\alpha)) = 0. \quad (75)$$

Ignoring the second order terms in the correction terms, we obtain to a first approximation

$$(\mathbf{F}\mathbf{x}'_\alpha, \Delta\mathbf{x}_\alpha) + (\mathbf{F}^\top \mathbf{x}_\alpha, \Delta\mathbf{x}'_\alpha) = (\mathbf{x}_\alpha, \mathbf{F}\mathbf{x}'_\alpha). \quad (76)$$

Since the correction terms $\Delta\mathbf{x}_\alpha$ and $\Delta\mathbf{x}'_\alpha$ are constrained to be in the image plane, we have the constraints

$$(\mathbf{k}, \Delta\mathbf{x}_\alpha) = 0, \quad (\mathbf{k}, \Delta\mathbf{x}'_\alpha) = 0, \quad (77)$$

where $\mathbf{k} \equiv (0, 0, 1)^\top$. Introducing Lagrange multipliers for (76) and (77), we obtain $\Delta\mathbf{x}_\alpha$ and $\Delta\mathbf{x}'_\alpha$ that minimize (74) as follows (see Appendix C):

$$\begin{aligned} \Delta\mathbf{x}_\alpha &= \frac{(\mathbf{x}_\alpha, \mathbf{F}\mathbf{x}'_\alpha) \mathbf{P}_\mathbf{k} \mathbf{F} \mathbf{x}'_\alpha}{(\mathbf{F}\mathbf{x}'_\alpha, \mathbf{P}_\mathbf{k} \mathbf{F} \mathbf{x}'_\alpha) + (\mathbf{F}^\top \mathbf{x}_\alpha, \mathbf{P}_\mathbf{k} \mathbf{F}^\top \mathbf{x}_\alpha)}, \\ \Delta\mathbf{x}'_\alpha &= \frac{(\mathbf{x}_\alpha, \mathbf{F}\mathbf{x}'_\alpha) \mathbf{P}_\mathbf{k} \mathbf{F}^\top \mathbf{x}_\alpha}{(\mathbf{F}\mathbf{x}'_\alpha, \mathbf{P}_\mathbf{k} \mathbf{F} \mathbf{x}'_\alpha) + (\mathbf{F}^\top \mathbf{x}_\alpha, \mathbf{P}_\mathbf{k} \mathbf{F}^\top \mathbf{x}_\alpha)}. \end{aligned} \quad (78)$$

Here, we define

$$\mathbf{P}_\mathbf{k} \equiv \text{diag}(1, 1, 0). \quad (79)$$

Substituting (78) into (74), we obtain (see Appendix C)

$$E = \sum_{\alpha=1}^N \frac{(\mathbf{x}_\alpha, \mathbf{F}\mathbf{x}'_\alpha)^2}{(\mathbf{F}\mathbf{x}'_\alpha, \mathbf{P}_\mathbf{k} \mathbf{F} \mathbf{x}'_\alpha) + (\mathbf{F}^\top \mathbf{x}_\alpha, \mathbf{P}_\mathbf{k} \mathbf{F}^\top \mathbf{x}_\alpha)}, \quad (80)$$

which is known as the *Sampson error* [7]. Suppose we have obtained the matrix \mathbf{F} that minimizes (80) subject to $\|\mathbf{F}\| = 1$ and $\det \mathbf{F} = 0$. Writing it as $\hat{\mathbf{F}}$ and substituting it into (78), we obtain

$$\begin{aligned}\hat{\mathbf{x}}_\alpha &= \mathbf{x}_\alpha - \frac{(\mathbf{x}_\alpha, \hat{\mathbf{F}}\mathbf{x}'_\alpha)\mathbf{P}_k\hat{\mathbf{F}}\mathbf{x}'_\alpha}{(\hat{\mathbf{F}}\mathbf{x}'_\alpha, \mathbf{P}_k\hat{\mathbf{F}}\mathbf{x}'_\alpha) + (\hat{\mathbf{F}}^\top\mathbf{x}_\alpha, \mathbf{P}_k\hat{\mathbf{F}}^\top\mathbf{x}_\alpha)}, \\ \hat{\mathbf{x}}'_\alpha &= \mathbf{x}'_\alpha - \frac{(\mathbf{x}_\alpha, \hat{\mathbf{F}}\mathbf{x}'_\alpha)\mathbf{P}_k\hat{\mathbf{F}}^\top\mathbf{x}_\alpha}{(\hat{\mathbf{F}}\mathbf{x}'_\alpha, \mathbf{P}_k\hat{\mathbf{F}}\mathbf{x}'_\alpha) + (\hat{\mathbf{F}}^\top\mathbf{x}_\alpha, \mathbf{P}_k\hat{\mathbf{F}}^\top\mathbf{x}_\alpha)}.\end{aligned}\quad (81)$$

Second approximation. The solution (81) is only a first approximation. So, we estimate the true solution $\bar{\mathbf{x}}_\alpha$ and $\bar{\mathbf{x}}'_\alpha$ by writing, instead of (73),

$$\bar{\mathbf{x}}_\alpha = \hat{\mathbf{x}}_\alpha - \Delta\hat{\mathbf{x}}_\alpha, \quad \bar{\mathbf{x}}'_\alpha = \hat{\mathbf{x}}'_\alpha - \Delta\hat{\mathbf{x}}'_\alpha, \quad (82)$$

and estimating the correction terms $\Delta\hat{\mathbf{x}}_\alpha$ and $\Delta\hat{\mathbf{x}}'_\alpha$, which are small quantities of higher order than $\Delta\mathbf{x}_\alpha$ and $\Delta\mathbf{x}'_\alpha$. Substitution of (82) into (71) yields

$$E = \sum_{\alpha=1}^N \left(\|\bar{\mathbf{x}}_\alpha + \Delta\hat{\mathbf{x}}_\alpha\|^2 + \|\bar{\mathbf{x}}'_\alpha + \Delta\hat{\mathbf{x}}'_\alpha\|^2 \right), \quad (83)$$

where we define

$$\bar{\mathbf{x}}_\alpha = \mathbf{x}_\alpha - \hat{\mathbf{x}}_\alpha, \quad \bar{\mathbf{x}}'_\alpha = \mathbf{x}'_\alpha - \hat{\mathbf{x}}'_\alpha. \quad (84)$$

The epipolar equation of (72) now becomes

$$(\hat{\mathbf{x}}_\alpha - \Delta\hat{\mathbf{x}}_\alpha, \mathbf{F}(\hat{\mathbf{x}}'_\alpha - \Delta\hat{\mathbf{x}}'_\alpha)) = 0. \quad (85)$$

Ignoring second order terms in $\Delta\hat{\mathbf{x}}_\alpha$ and $\Delta\hat{\mathbf{x}}'_\alpha$, which are already of high order, we have

$$(\mathbf{F}\hat{\mathbf{x}}'_\alpha, \Delta\hat{\mathbf{x}}_\alpha) + (\mathbf{F}^\top\hat{\mathbf{x}}_\alpha, \Delta\hat{\mathbf{x}}'_\alpha) = (\hat{\mathbf{x}}_\alpha, \mathbf{F}\hat{\mathbf{x}}'_\alpha). \quad (86)$$

This is a higher order approximation of (72) than (76). Introducing Lagrange multipliers to (86) and the constraints

$$(\mathbf{k}, \Delta\hat{\mathbf{x}}_\alpha) = 0, \quad (\mathbf{k}, \Delta\hat{\mathbf{x}}'_\alpha) = 0, \quad (87)$$

we obtain $\Delta\hat{\mathbf{x}}_\alpha$ and $\Delta\hat{\mathbf{x}}'_\alpha$ that minimize (80) as follows (see Appendix C):

$$\begin{aligned}\Delta\hat{\mathbf{x}}_\alpha &= \frac{\left((\hat{\mathbf{x}}_\alpha, \mathbf{F}\hat{\mathbf{x}}'_\alpha) + (\mathbf{F}\hat{\mathbf{x}}'_\alpha, \tilde{\mathbf{x}}_\alpha) + (\mathbf{F}^\top\hat{\mathbf{x}}_\alpha, \tilde{\mathbf{x}}'_\alpha) \right) \mathbf{P}_k\mathbf{F}\hat{\mathbf{x}}'_\alpha}{(\mathbf{F}\hat{\mathbf{x}}'_\alpha, \mathbf{P}_k\mathbf{F}\hat{\mathbf{x}}'_\alpha) + (\mathbf{F}^\top\hat{\mathbf{x}}_\alpha, \mathbf{P}_k\mathbf{F}^\top\hat{\mathbf{x}}_\alpha)} \\ &\quad - \tilde{\mathbf{x}}_\alpha, \\ \Delta\hat{\mathbf{x}}'_\alpha &= \frac{\left((\hat{\mathbf{x}}_\alpha, \mathbf{F}\hat{\mathbf{x}}'_\alpha) + (\mathbf{F}\hat{\mathbf{x}}'_\alpha, \tilde{\mathbf{x}}_\alpha) + (\mathbf{F}^\top\hat{\mathbf{x}}_\alpha, \tilde{\mathbf{x}}'_\alpha) \right) \mathbf{P}_k\mathbf{F}^\top\hat{\mathbf{x}}_\alpha}{(\mathbf{F}\hat{\mathbf{x}}'_\alpha, \mathbf{P}_k\mathbf{F}\hat{\mathbf{x}}'_\alpha) + (\mathbf{F}^\top\hat{\mathbf{x}}_\alpha, \mathbf{P}_k\mathbf{F}^\top\hat{\mathbf{x}}_\alpha)} \\ &\quad - \tilde{\mathbf{x}}'_\alpha.\end{aligned}\quad (88)$$

On substitution of (88), the reprojection error E now has the following form (see Appendix C):

$$E = \sum_{\alpha=1}^N \frac{\left((\hat{\mathbf{x}}_\alpha, \mathbf{F}\hat{\mathbf{x}}'_\alpha) + (\mathbf{F}\hat{\mathbf{x}}'_\alpha, \tilde{\mathbf{x}}_\alpha) + (\mathbf{F}^\top\hat{\mathbf{x}}_\alpha, \tilde{\mathbf{x}}'_\alpha) \right)^2}{(\mathbf{F}\hat{\mathbf{x}}'_\alpha, \mathbf{P}_k\mathbf{F}\hat{\mathbf{x}}'_\alpha) + (\mathbf{F}^\top\hat{\mathbf{x}}_\alpha, \mathbf{P}_k\mathbf{F}^\top\hat{\mathbf{x}}_\alpha)}. \quad (89)$$

Suppose we have obtained the matrix \mathbf{F} that minimizes this subject to $\|\mathbf{F}\| = 1$ and $\det \mathbf{F} = 0$. Writing it as $\hat{\mathbf{F}}$ and substituting it into (88), we obtain the solution

$$\begin{aligned}\hat{\hat{\mathbf{x}}}_\alpha &= \mathbf{x}_\alpha \\ &\quad - \frac{\left((\hat{\mathbf{x}}_\alpha, \hat{\mathbf{F}}\hat{\mathbf{x}}'_\alpha) + (\hat{\mathbf{F}}\hat{\mathbf{x}}'_\alpha, \tilde{\mathbf{x}}_\alpha) + (\hat{\mathbf{F}}^\top\hat{\mathbf{x}}_\alpha, \tilde{\mathbf{x}}'_\alpha) \right) \mathbf{P}_k\hat{\mathbf{F}}\hat{\mathbf{x}}'_\alpha}{(\hat{\mathbf{F}}\hat{\mathbf{x}}'_\alpha, \mathbf{P}_k\hat{\mathbf{F}}\hat{\mathbf{x}}'_\alpha) + (\hat{\mathbf{F}}^\top\hat{\mathbf{x}}_\alpha, \mathbf{P}_k\hat{\mathbf{F}}^\top\hat{\mathbf{x}}_\alpha)}, \\ \hat{\hat{\mathbf{x}}}'_\alpha &= \mathbf{x}'_\alpha \\ &\quad - \frac{\left((\hat{\mathbf{x}}_\alpha, \hat{\mathbf{F}}\hat{\mathbf{x}}'_\alpha) + (\hat{\mathbf{F}}\hat{\mathbf{x}}'_\alpha, \tilde{\mathbf{x}}_\alpha) + (\hat{\mathbf{F}}^\top\hat{\mathbf{x}}_\alpha, \tilde{\mathbf{x}}'_\alpha) \right) \mathbf{P}_k\hat{\mathbf{F}}^\top\hat{\mathbf{x}}_\alpha}{(\hat{\mathbf{F}}\hat{\mathbf{x}}'_\alpha, \mathbf{P}_k\hat{\mathbf{F}}\hat{\mathbf{x}}'_\alpha) + (\hat{\mathbf{F}}^\top\hat{\mathbf{x}}_\alpha, \mathbf{P}_k\hat{\mathbf{F}}^\top\hat{\mathbf{x}}_\alpha)}.\end{aligned}\quad (90)$$

The resulting $\{\hat{\hat{\mathbf{x}}}_\alpha, \hat{\hat{\mathbf{x}}}'_\alpha\}$ are a better approximation than $\{\hat{\mathbf{x}}_\alpha, \hat{\mathbf{x}}'_\alpha\}$. Rewriting $\{\hat{\hat{\mathbf{x}}}_\alpha, \hat{\hat{\mathbf{x}}}'_\alpha\}$ as $\{\hat{\mathbf{x}}_\alpha, \hat{\mathbf{x}}'_\alpha\}$, we can estimate a yet better solution in the form of (82). We repeat this until the iterations converge.

Fundamental matrix computation. The remaining problem is to compute the matrix \mathbf{F} that minimizes (80) and (89) subject to $\|\mathbf{F}\| = 1$ and $\det \mathbf{F} = 0$. If we use the representation in (3) and (4), we can confirm the identities

$$(\mathbf{x}_\alpha, \mathbf{F}\mathbf{x}'_\alpha) = \frac{(\mathbf{u}, \boldsymbol{\xi}_\alpha)}{f_0^2}, \quad (91)$$

$$(\mathbf{F}\mathbf{x}'_\alpha, \mathbf{P}_k\mathbf{F}\mathbf{x}'_\alpha) + (\mathbf{F}^\top\mathbf{x}_\alpha, \mathbf{P}_k\mathbf{F}^\top\mathbf{x}_\alpha) = \frac{(\mathbf{u}, V_0[\boldsymbol{\xi}_\alpha]\mathbf{u})}{f_0^2}, \quad (92)$$

where $V_0[\boldsymbol{\xi}_\alpha]$ is the matrix in (7). Using (91) and (92), the reprojection error E in (80) can be written as

$$E = \frac{1}{f_0^2} \sum_{\alpha=1}^N \frac{(\mathbf{u}, \boldsymbol{\xi}_\alpha)^2}{(\mathbf{u}, V_0[\boldsymbol{\xi}_\alpha]\mathbf{u})}, \quad (93)$$

which is identical to (14) except the scale. The matrix \mathbf{F} that minimizes (93) subject to $\|\mathbf{F}\| = 1$ and $\det \mathbf{F} = 0$ can be determined by the methods described in Sections 3–5.

Now, if we define

$$\hat{\xi}_\alpha = \begin{pmatrix} \hat{x}_\alpha \hat{x}'_\alpha + \hat{x}'_\alpha \tilde{x}_\alpha + \hat{x}_\alpha \tilde{x}'_\alpha \\ \hat{x}_\alpha \hat{y}'_\alpha + \hat{y}'_\alpha \tilde{x}_\alpha + \hat{x}_\alpha \tilde{y}'_\alpha \\ f_0(\hat{x}_\alpha + \tilde{x}_\alpha) \\ \hat{y}_\alpha \hat{x}'_\alpha + \hat{x}'_\alpha \hat{y}_\alpha + \hat{y}_\alpha \tilde{x}'_\alpha \\ \hat{y}_\alpha \hat{y}'_\alpha + \hat{y}'_\alpha \hat{y}_\alpha + \hat{y}_\alpha \tilde{y}'_\alpha \\ f_0(\hat{y}_\alpha + \tilde{y}_\alpha) \\ f_0(\hat{x}'_\alpha + \tilde{x}'_\alpha) \\ f_0(\hat{y}'_\alpha + \tilde{y}'_\alpha) \\ f_0^2 \end{pmatrix}, \quad (94)$$

we can confirm the identities

$$(\hat{x}_\alpha, \hat{\mathbf{F}} \hat{x}'_\alpha) + (\hat{\mathbf{F}} \hat{x}'_\alpha, \tilde{x}_\alpha) + (\hat{\mathbf{F}}^\top \hat{x}_\alpha, \tilde{x}'_\alpha) = \frac{(\mathbf{u}, \hat{\xi}_\alpha)}{f_0^2}, \quad (95)$$

$$(\hat{\mathbf{F}} \mathbf{x}'_\alpha, \mathbf{P}_k \hat{\mathbf{F}} \mathbf{x}'_\alpha) + (\hat{\mathbf{F}}^\top \mathbf{x}_\alpha, \mathbf{P}_k \hat{\mathbf{F}}^\top \mathbf{x}_\alpha) = \frac{(\mathbf{u}, V_0[\hat{\xi}_\alpha] \mathbf{u})}{f_0^2}, \quad (96)$$

where $V_0[\hat{\xi}_\alpha]$ is the matrix obtained by replacing x_α , y_α , x'_α , and y'_α in (7) by \hat{x}_α , \hat{y}'_α , \tilde{x}'_α , and \tilde{y}'_α , respectively. Hence, (89) is rewritten as

$$E = \frac{1}{f_0^2} \sum_{\alpha=1}^N \frac{(\mathbf{u}, \hat{\xi}_\alpha)^2}{(\mathbf{u}, V_0[\hat{\xi}_\alpha] \mathbf{u})}, \quad (97)$$

which is again identical to (14) in form except the scale; if $\hat{x}_\alpha = x_\alpha$, the vector $\hat{\xi}_\alpha$ in (94) reduces to ξ_α , and (97) reduces to (93). Thus, the matrix \mathbf{F} that minimizes (97) subject to $\|\mathbf{F}\| = 1$ and $\det \mathbf{F} = 0$ can be determined by the methods in Sections 3–5. *This is the core discovery of this paper*, unnoticed in the past.

Procedure. Our bundle adjustment computation is summarized as follows.

1. Let $\mathbf{u}_0 = \mathbf{0}$.
2. Let $\hat{x}_\alpha = x_\alpha$, $\hat{y}_\alpha = y_\alpha$, $\hat{x}'_\alpha = x'_\alpha$, $\hat{y}'_\alpha = y'_\alpha$, and $\tilde{x}_\alpha = \tilde{y}_\alpha = \tilde{x}'_\alpha = \tilde{y}'_\alpha = 0$.
3. Compute the vectors $\hat{\xi}_\alpha$ and the matrices $V_0[\hat{\xi}_\alpha]$.
4. Compute the vector \mathbf{u} that minimizes

$$E = \frac{1}{f_0^2} \sum_{\alpha=1}^N \frac{(\mathbf{u}, \hat{\xi}_\alpha)^2}{(\mathbf{u}, V_0[\hat{\xi}_\alpha] \mathbf{u})}, \quad (98)$$

subject to $\|\mathbf{u}\| = 1$ and $(\mathbf{u}^\dagger, \mathbf{u}) = 0$.

5. If $\mathbf{u} \approx \mathbf{u}_0$ up to sign, return \mathbf{u} and stop. Else, update \tilde{x}_α , \tilde{y}_α , \tilde{x}'_α , and \tilde{y}'_α as follows:

$$\tilde{x}_\alpha \leftarrow \frac{(\mathbf{u}, \hat{\xi}_\alpha) \mathbf{P}_k \hat{\mathbf{F}} \hat{x}'_\alpha}{(\mathbf{u}, V_0[\hat{\xi}_\alpha] \mathbf{u})}, \quad \tilde{x}'_\alpha \leftarrow \frac{(\mathbf{u}, \hat{\xi}_\alpha) \mathbf{P}_k \hat{\mathbf{F}}^\top \hat{x}_\alpha}{(\mathbf{u}, V_0[\hat{\xi}_\alpha] \mathbf{u})}. \quad (99)$$

6. Go back to Step 3 after the following update:

$$\begin{aligned} \mathbf{u}_0 &\leftarrow \mathbf{u}, & \hat{x}_\alpha &\leftarrow x_\alpha - \tilde{x}_\alpha, & \hat{y}_\alpha &\leftarrow y_\alpha - \tilde{y}_\alpha, \\ \hat{x}'_\alpha &\leftarrow x'_\alpha - \tilde{x}'_\alpha, & \hat{y}'_\alpha &\leftarrow y'_\alpha - \tilde{y}'_\alpha. \end{aligned} \quad (100)$$

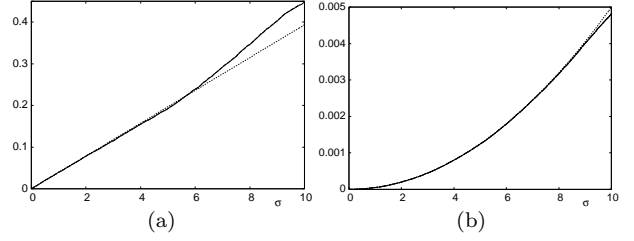


Figure 14: (a) The RMS errors for Fig. 3. Dashed line: Sampson solution. Solid line: Gold Standard solution. Dotted line: KCR lower bound. The dashed line and the solid line practically coincide. (b) The average reprojection error for Fig. 3. Chained line: Sampson error. Dashed line: Sampson reprojection error. Solid line: Gold Standard error. Dotted line: $(N-7)\sigma^2/f_0^2$. The chained line, the dashed line, and the solid line practically coincide.

8. Effect of Bundle Adjustment

The above computation reduces to the Mahalanobis distance minimization in the ξ -space if we stop at Step 5. So, the issue is how the accuracy improves by the subsequent iterations. Borrowing the terminology of Hartley and Zisserman [7], let us call the solution obtained at Step 5 the *Sampson solution* and the solution obtained after the iterations the *Gold Standard solution*.

Simulations. Using the simulated images in Figs. 3 and 9, we computed the RMS error D in (70) over 10000 trials. Figs. 14(a) and 15(a) correspond to Figs. 8 and 14, respectively, except that the horizontal axis is now extended to an extremely large noise level.

For minimizing (98), we used EFNS initialized by the Taubin method at fist; in the next round and thereafter, the solution in the preceding round is used to start the EFNS. If the EFNS iterations did not converge after 100 iterations, which sometimes occurs in an extremely large noise range, we switched to the projective Gauss-Newton iterations followed by optimal correction followed by the 7-parameter LM search. We did preliminary experiments for testing the convergence properties of FNS, HEIV, projective Gauss-Newton iterations, and EFNS and found that projective Gauss-Newton iterations and EFNS can tolerate larger noise than others.

Figs. 14(b) and 15(b) compare the reprojection error of the two solutions. The chained line shows the average (over 10000 trials) of the reprojection error in (98) in the first round; we call it the *Sampson error*. The solid line shows the average of the value resulting in the final round; we call it the *Gold Standard error*.

To compute the reprojection error of the Sampson solution, which we call the *Sampson reprojection error*, we minimized E in (71) with respect to \bar{x}_α and \bar{x}'_α , $\alpha = 1, \dots, N$, subject to (72) with the computed \mathbf{F} fixed; the computation goes the same as described

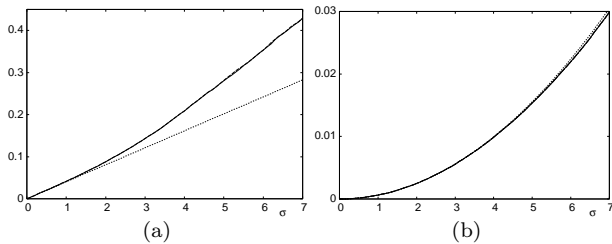


Figure 15: (a) The RMS errors for Fig. 9. Dashed line: Sampson solution. Solid line: Gold Standard solution. Dotted line: KCR lower bound. The solid line is very slightly below the dashed line for $\sigma > 5$. (b) The average reprojection error for Fig. 9. Chained line: Sampson error. Dashed line: Sampson reprojection error. Solid line: Gold Standard error. Dotted line: $(N - 7)\sigma^2/f_0^2$. The chained line, the dashed line, and the solid line practically coincide.

in the preceding section except that \mathbf{F} is fixed. The dashed line shows the average of the resulting Sampson reprojection errors.

Observations. As can be seen from Figs. 14(a) and 15(a), the RMS errors of the Sampson and the Gold Standard solutions virtually coincide. In Fig. 15(b), we see that the Gold Standard solution *does* have a very slightly smaller RMS error for σ larger than 5, but the difference is too small to be significant in view of the statistical nature of the problem.

From Fig. 14(b) and 15(b), we see that the Sampson error, the Sampson reprojection error, and the Gold Standard error are practically identical; they are all very close to the first order estimate $(N - 7)\sigma^2/f_0^2$. Theoretically, the Gold Standard error should be smaller than the Sampson reprojection error, because we add higher order correction. This is *indeed so*, but the difference is too small to be visible in the plot.

Let us call the computed fundamental matrix *meaningful* if its relative error is less than 50%. Certainly, we cannot expect meaningful applications of camera calibration or 3-D reconstruction if the computed fundamental matrix has 50% or larger errors. We can see that Figs. 14 and 15 nearly covers the noise level range for which meaningful estimation is possible (recall that the solution is normalized to unit norm, so the RMS error roughly corresponds to the relative error).

If the noise is very large, the objective function becomes very flat around its minimum, so large deviations are inevitable whatever computational method is used; the KCR lower bound exactly describes this situation. From such a flat distribution, we may sometimes observe a solution very close to the true value and other times a very wrong one. So, the accuracy evaluation must be done with a large number of trials. In fact, we observed that the RMS error plots of the Sampson and the Gold Standard solutions were visibly different with 1000 trials for each σ . However,

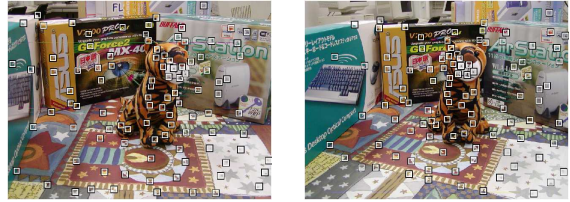


Figure 16: Real images and 100 corresponding points.

Table 1: Residuals and execution times (sec).

method	residual	time
SVD-corrected LS	45.550	.00052
SVD-corrected ML	45.556	.00652
CFNS	45.556	.01300
opt. corrected ML	45.378	.00764
7-LM from LS	45.378	.01136
7-LM from opt. corrected ML	45.378	.01748
EFNS	45.379	.01916
bundle adjustment	45.379	.02580

they practically coincided after 10000 trials. In the past, a hasty conclusion was often drawn after a few experiments. Doing many experiments, we failed to observe that the Gold Standard solution is any better than the Sampson solution, quite contrary to the assertion by Hartley and Zisserman [7].

Real image example. We manually selected 100 pairs of corresponding points in the two images in Fig. 16 and computed the fundamental matrix from them. The final residual \hat{J} (= the minimum of (14)) and the execution time (sec) are listed in Table 1. We used Core2Duo E6700 2.66GHz for the CPU with 4GB main memory and Linux for the OS.

We can see that for this example optimally corrected ML, 7-parameter LM (abbr. 7-LM) started from either LS or optimally corrected ML, EFNS, and bundle adjustment all converged to the same solution, indicating that all are optimal. The Gold Standard error coincides with the Sampson error up to five significant digits. We can also see that SVD-corrected LS (Hartley’s 8-point method) and SVD-corrected ML have higher residual than the optimal solution and that CFNS has as high a residual as SVD-corrected ML.

9. Conclusions

We categorized algorithms for computing the fundamental matrix from point correspondences into “a posteriori correction”, “internal access”, and “external access” and reviewed existing methods in this framework. Then, we proposed new schemes¹³:

1. a new internal access method: 7-parameter LM

¹³Source codes are available at <http://www.iim.ics.tut.ac.jp/~sugaya/public-e.html>

search.

2. a new external access method: EFNS.
3. a new EFNS-based bundle adjustment algorithm.

We conducted experimental comparison and observed that the popular SVD-corrected LS (Hartley's 8-point algorithm) has poor performance. We also observed that the CFNS of Chojnacki et al. [4], a pioneering external access method, does not necessarily converge to a correct solution, while our EFNS always yields an optimal value; we gave a mathematical justification to this.

After many experiments (not all shown here), we concluded that EFNS and the 7-parameter LM search started from optimally corrected ML exhibited the best performance. We also observed that additional bundle adjustment (Gold Standard) does not increase the accuracy to any noticeable degree.

Acknowledgments: This work was done in part in collaboration with Mitsubishi Precision, Co. Ltd., Japan. The authors thank Mike Brooks, Wojciech Chojnacki, and Anton van den Hengel of the University Adelaide, Australia, for providing software and helpful discussions. They also thank Nikolai Chernov of the University of Alabama at Birmingham, U.S.A. for helpful discussions.

References

- [1] A. Bartoli and P. Sturm, "Nonlinear estimation of fundamental matrix with minimal parameters," *IEEE Trans. Pattern Analysis and Machine Intelligence*, vol. 26, no. 3, pp. 426–432, March 2004.
- [2] N. Chernov and C. Lesort, "Statistical efficiency of curve fitting algorithms," *Computational Statistics and Data Analysis*, vol. 47, no. 4, pp. 713–728, November 2004.
- [3] W. Chojnacki, M.J. Brooks, A. van den Hengel and D. Gawley, "On the fitting of surfaces to data with covariances," *IEEE Trans. Pattern Analysis and Machine Intelligence*, vol. 22, no. 11, pp. 1294–1303, November 2000.
- [4] W. Chojnacki, M.J. Brooks, A. van den Hengel and D. Gawley, "A new constrained parameter estimator for computer vision applications," *Image and Vision Computing*, vol. 22, no. 2, pp. 85–91, February 2004.
- [5] W. Chojnacki, M.J. Brooks, A. van den Hengel, and D. Gawley, "FNS, CFNS and HEIV: A unifying approach," *J. Mathematical Imaging and Vision*, vol. 23, no. 2, pp. 175–183, 2005-9)
- [6] R.I. Hartley, "In defense of the eight-point algorithm," *IEEE Trans. Pattern Analysis and Machine Intelligence*, vol. 19, no. 6, pp. 580–593, 1997-6)
- [7] R. Hartley and A. Zisserman, *Multiple View Geometry in Computer Vision*. Cambridge University Press, Cambridge, U.K., 2000.
- [8] C. Harris and M. Stephens, "A combined corner and edge detector," *Proc. 4th Alvey Vision Conf.*, pp. 147–151, August 1988.
- [9] K. Kanatani, *Group-Theoretical Methods in Image Understanding*. Springer, Berlin, 1990.
- [10] K. Kanatani, *Statistical Optimization for Geometric Computation: Theory and Practice*. Elsevier Science, Amsterdam, The Netherlands, 1996; reprinted, Dover, New York, 2005.
- [11] K. Kanatani, "Ellipse fitting with hyperaccuracy," *IEICE Trans. Information and Systems*, vol. E89-D, no. 10, pp. 2653–2660, October 2006.
- [12] K. Kanatani, "Statistical optimization for geometric fitting: Theoretical accuracy bound and high order error analysis," *Int'l J. Computer Vision*, to appear.
- [13] K. Kanatani and Y. Sugaya, "High accuracy fundamental matrix computation and its performance evaluation," *IEICE Trans. Information and Systems*, vol. E90-D, no. 2, pp. 579–585, February 2007.
- [14] K. Kanatani and Y. Sugaya, "Extended FNS for constrained parameter estimation," *Proc. 10th Meeting Image Recognition and Understanding*, pp. 219–226, July 2007.
- [15] Y. Kanazawa and K. Kanatani "Robust image matching preserving global consistency," *Proc. 6th Asian Conf. Computer Vision*, pp. 1128–1133, January 2004.
- [16] Y. Leedan and P. Meer, "Heteroscedastic regression in computer vision: Problems with bilinear constraint," *Int'l J. Computer Vision*, vol. 37, no. 2, pp. 127–150, June 2000.
- [17] D.G. Lowe, "Distinctive image features from scale-invariant keypoints," *Int'l J. Computer Vision*, vol. 60, no. 2, pp. 91–110, November 2004.
- [18] J. Matei and P. Meer, "Estimation of nonlinear errors-in-variables models for computer vision applications," *IEEE Trans. Pattern Analysis and Machine Intelligence*, vol. 28, no. 10, pp. 1537–1552, October 2006.
- [19] J. Matasu, O. Chum, M. Urban, and T. Pajdla, "Robust wide-baseline stereo from maximally stable extremal regions," *Image and Vision Computing*, vol. 22, no. 10, pp. 761–767, September 2004.
- [20] K. Mikolajczyk and C. Schmidt, "Scale and affine invariant interest point detectors," *Int'l J. Computer Vision*, vol. 60, no. 1, pp. 63–86, October 2004.
- [21] P. Meer, "Robust techniques for computer vision," in G. Medioni and S. B. Kang (Eds.), *Emerging Topics in Computer Vision*. Prentice Hall, Upper Saddle River, NJ, U.S.A., 2004, pp. 107–190.
- [22] T. Migita and T. Shakunaga, "One-dimensional search for reliable epipole estimation," *Proc. IEEE Pacific Rim Symp. Image and Video Technology*, pp. 1215–1224, December 2006.
- [23] S.M. Smith and J.M. Brady, "SUSAN—A new approach to low level image processing," *Int'l J. Computer Vision*, vol. 23, no. 1, pp. 45–78, January 1997.
- [24] Y. Sugaya and K. Kanatani, "High accuracy computation of rank-constrained fundamental matrix," *Proc. 18th British Machine Vision Conf.*, vol. 1, pp. 282–291, September 2007.
- [25] Y. Sugaya and K. Kanatani, "Highest accuracy fundamental matrix computation," *Proc. 8th Asian Conf. Computer Vision*, November 2008, to appear.
- [26] G. Taubin, "Estimation of planar curves, surfaces, and non-planar space curves defined by implicit equations with applications to edge and range image segmentation," *IEEE Trans. Pattern Analysis and Machine Intelligence*, vol. 13, no. 11, pp. 1115–1138, November 1991.

- [27] Z. Zhang, R. Deriche, O. Faugeras and Q.-T. Luong, "A robust technique for matching two uncalibrated images through the recovery of the unknown epipolar geometry," *Artificial Intelligence*, vol. 78, pp. 87–119, 1995.
- [28] Z. Zhang and C. Loop, "Estimating the fundamental matrix by transforming image points in projective space," *Computer Vision and Image Understanding*, vol. 82, no. 2, pp. 174–180, May 2001.

Appendix

A. Derivation of the 6-parameter LM

First, note that if \mathbf{F} has the form of (47), we see that

$$\begin{aligned}\|\mathbf{F}\|^2 &= \sum_{i,j=1}^3 F_{ij}^2 = \text{tr}[\mathbf{F}\mathbf{F}^\top] \\ &= \text{tr}[\mathbf{U}\text{diag}(\sigma_1, \sigma_2, 0)\mathbf{V}^\top\mathbf{V}\text{diag}(\sigma_1, \sigma_2, 0)\mathbf{U}^\top] \\ &= \text{tr}[\mathbf{U}^\top\mathbf{U}\text{diag}(\sigma_1^2, \sigma_2^2, 0)] = \sigma_1^2 + \sigma_2^2,\end{aligned}\quad (101)$$

where we have used the matrix identity $\text{tr}[\mathbf{A}\mathbf{B}] = \text{tr}[\mathbf{B}\mathbf{A}]$ together with the orthogonality $\mathbf{V}^\top\mathbf{V} = \mathbf{I}$ and $\mathbf{U}^\top\mathbf{U} = \mathbf{I}$. Thus, the parameterization of (48) ensures the normalization $\|\mathbf{F}\| = 1$.

Suppose the orthogonal matrices \mathbf{U} and \mathbf{V} undergo a small change into $\mathbf{U} + \Delta\mathbf{U}$ and $\mathbf{V} + \Delta\mathbf{V}$, respectively. According to the Lie group theory [9], there exist small vectors $\boldsymbol{\omega}$ and $\boldsymbol{\omega}'$ such that the increments $\Delta\mathbf{U}$ and $\Delta\mathbf{V}$ are written as

$$\Delta\mathbf{U} = \boldsymbol{\omega} \times \mathbf{U}, \quad \Delta\mathbf{V} = \boldsymbol{\omega}' \times \mathbf{V} \quad (102)$$

to a first approximation, where the operator \times means column-wise vector product. It follows that the increment $\Delta\mathbf{F}$ in \mathbf{F} is written to a first approximation as

$$\begin{aligned}\Delta\mathbf{F} &= \boldsymbol{\omega} \times \mathbf{U}\text{diag}(\cos\theta, \sin\theta, 0)\mathbf{V}^\top \\ &\quad + \mathbf{U}\text{diag}(-\sin\theta\Delta\theta, \cos\theta\Delta\theta, 0)\mathbf{V}^\top \\ &\quad + \mathbf{U}\text{diag}(\cos\theta, \sin\theta, 0)(\boldsymbol{\omega}' \times \mathbf{V})^\top.\end{aligned}\quad (103)$$

Taking out the elements, we can rearrange this in the vector form

$$\Delta\mathbf{u} = \mathbf{F}_U\boldsymbol{\omega} + \mathbf{u}_\theta\Delta\theta + \mathbf{F}_V\boldsymbol{\omega}', \quad (104)$$

where \mathbf{F}_U and \mathbf{F}_V are the matrices in (50) and \mathbf{u}_θ is defined by (52). The resulting increment ΔJ in J is written to a first approximation as

$$\begin{aligned}\Delta J &= (\nabla_{\mathbf{u}}J, \Delta\mathbf{u}) = (2\mathbf{X}\mathbf{u}, \mathbf{F}_U\boldsymbol{\omega} + \mathbf{u}_\theta\Delta\theta + \mathbf{F}_V\boldsymbol{\omega}') \\ &= 2(\mathbf{F}_U^\top\mathbf{X}\mathbf{u}, \boldsymbol{\omega}) + 2(\mathbf{u}_\theta, \mathbf{X}\mathbf{u})\Delta\theta \\ &\quad + 2(\mathbf{F}_V^\top\mathbf{X}\mathbf{u}, \boldsymbol{\omega}'),\end{aligned}\quad (105)$$

which shows that the first derivatives of J are given by (49) and (51). The second order increment is

$$\Delta^2 J = (\Delta\mathbf{u}, \nabla_{\mathbf{u}}^2 J \Delta\mathbf{u})$$

$$\begin{aligned}&= (\mathbf{F}_U\boldsymbol{\omega} + \mathbf{u}_\theta\Delta\theta + \mathbf{F}_V\boldsymbol{\omega}', 2\mathbf{M}(\mathbf{F}_U\boldsymbol{\omega} + \mathbf{u}_\theta\Delta\theta \\ &\quad + \mathbf{F}_V\boldsymbol{\omega}')) \\ &= 2(\boldsymbol{\omega}, \mathbf{F}_U^\top\mathbf{M}\mathbf{F}_U\boldsymbol{\omega}) + 2(\boldsymbol{\omega}', \mathbf{F}_V^\top\mathbf{M}\mathbf{F}_V\boldsymbol{\omega}') \\ &\quad + 2(\mathbf{u}_\theta, \mathbf{M}\mathbf{u}_\theta)\Delta\theta^2 + 4(\boldsymbol{\omega}, \mathbf{F}_U^\top\mathbf{M}\boldsymbol{\omega}') \\ &\quad + 4(\boldsymbol{\omega}, \mathbf{F}_U^\top\mathbf{M}\mathbf{u}_\theta)\Delta\theta + 4(\boldsymbol{\omega}', \mathbf{F}_V^\top\mathbf{M}\mathbf{u}_\theta)\Delta\theta,\end{aligned}\quad (106)$$

where we have used the Gauss-Newton approximation $\nabla_{\mathbf{u}}^2 J \approx 2\mathbf{M}$. From this, we obtain the second derivatives in (53).

B. Details of CFNS

According to Chojnacki et al. [4], the matrix \mathbf{Q} in (62) is given without any reasoning as follows (their original symbols are altered to conform to the use in this paper). The gradient $\nabla_{\mathbf{u}}J = (\partial J/\partial u_i)$ and the Hessian $\nabla_{\mathbf{u}}^2 J = (\partial^2 J/\partial u_i \partial u_j)$ of (14) are

$$\nabla_{\mathbf{u}}J = 2(\mathbf{M} - \mathbf{L})\mathbf{u}, \quad \nabla_{\mathbf{u}}^2 J = 2(\mathbf{M} - \mathbf{L}) - 8(\mathbf{S} - \mathbf{T}), \quad (107)$$

where \mathbf{M} and \mathbf{L} are the matrices in (21), and we define

$$\begin{aligned}\mathbf{S} &= \sum_{\alpha=1}^N \frac{(\mathbf{u}, \boldsymbol{\xi}_\alpha)\mathcal{S}[\boldsymbol{\xi}_\alpha(V_0[\boldsymbol{\xi}_\alpha]\mathbf{u})^\top]}{(\mathbf{u}, V_0[\boldsymbol{\xi}_\alpha]\mathbf{u})^2}, \\ \mathbf{T} &= \sum_{\alpha=1}^N \frac{(\mathbf{u}, \boldsymbol{\xi}_\alpha)^2(V_0[\boldsymbol{\xi}_\alpha]\mathbf{u})(V_0[\boldsymbol{\xi}_\alpha]\mathbf{u}^\top)^\top}{(\mathbf{u}, V_0[\boldsymbol{\xi}_\alpha]\mathbf{u})^3}.\end{aligned}\quad (108)$$

Here, $\mathcal{S}[\cdot]$ is the symmetrization operator ($\mathcal{S}[\mathbf{A}] = (\mathbf{A} + \mathbf{A}^\top)/2$). Let

$$\begin{aligned}\mathbf{A} &= \mathbf{P}_{\mathbf{u}^\dagger}(\nabla_{\mathbf{u}}^2 J)(2\mathbf{u}\mathbf{u}^\top - \mathbf{I}), \\ \mathbf{B} &= \frac{2}{\|\det \mathbf{u}\|} \left(\sum_{i=1}^9 \mathcal{S}[(\nabla_{\mathbf{u}}^2 \det \mathbf{u})\mathbf{e}_i]\mathbf{u}^{\dagger\top}(\nabla_{\mathbf{u}}J)\mathbf{e}_i^\top \right. \\ &\quad \left. - (\mathbf{u}^\dagger, \nabla_{\mathbf{u}}J)\mathbf{u}^\dagger\mathbf{u}^{\dagger\top}\nabla_{\mathbf{u}}^2 \det \mathbf{u} \right), \\ \mathbf{C} &= 3 \left(\frac{\det \mathbf{u}}{\|\nabla_{\mathbf{u}} \det \mathbf{u}\|^2} \nabla_{\mathbf{u}}^2 \det \mathbf{u} \right. \\ &\quad \left. + \mathbf{u}^\dagger\mathbf{u}^{\dagger\top} \left(\mathbf{I} - \frac{2 \det \mathbf{u}}{\|\nabla_{\mathbf{u}} \det \mathbf{u}\|^2} \nabla_{\mathbf{u}}^2 \det \mathbf{u} \right) \right),\end{aligned}\quad (109)$$

where \mathbf{u}^\dagger is the cofactor vector of \mathbf{u} , $\mathbf{P}_{\mathbf{u}^\dagger}$ is the projection matrix in (58), and \mathbf{e}_i is the i th coordinate basis vector (with 0 components except 1 in the i th position). The matrix \mathbf{Q} is given by

$$\mathbf{Q} = (\mathbf{A} + \mathbf{B} + \mathbf{C})(\mathbf{A} + \mathbf{B} + \mathbf{C})^\top. \quad (110)$$

C. Details of bundle adjustment

Introducing Lagrange multipliers λ_α , μ_α , and μ'_α for the constraints of (76), and (77) to (74), we let

$$L = \sum_{\alpha=1}^N \left(\|\Delta\mathbf{x}_\alpha\|^2 + \|\Delta\mathbf{x}'_\alpha\|^2 \right)$$

$$\begin{aligned} & - \sum_{\alpha=1}^N \lambda_{\alpha} \left((\mathbf{F}\mathbf{x}'_{\alpha}, \Delta\mathbf{x}_{\alpha}) + (\mathbf{F}^{\top}\mathbf{x}_{\alpha}, \Delta\mathbf{x}'_{\alpha}) \right) \\ & - \sum_{\alpha=1}^N \mu_{\alpha}(\mathbf{k}, \Delta\mathbf{x}_{\alpha}) - \sum_{\alpha=1}^N \mu'_{\alpha}(\mathbf{k}, \Delta\mathbf{x}'_{\alpha}). \end{aligned} \quad (111)$$

Letting the derivatives of L with respect to $\Delta\mathbf{x}_{\alpha}$ and $\Delta\mathbf{x}'_{\alpha}$ be $\mathbf{0}$, we have

$$\begin{aligned} 2\Delta\mathbf{x}_{\alpha} - \lambda_{\alpha}\mathbf{F}\mathbf{x}'_{\alpha} - \mu_{\alpha}\mathbf{k} &= \mathbf{0}, \\ 2\Delta\mathbf{x}'_{\alpha} - \lambda_{\alpha}\mathbf{F}^{\top}\mathbf{x}_{\alpha} - \mu'_{\alpha}\mathbf{k} &= \mathbf{0}. \end{aligned} \quad (112)$$

Multiplying the projection matrix $\mathbf{P}_{\mathbf{k}}$ in (79) on both sides from left and noting that $\mathbf{P}_{\mathbf{k}}\Delta\mathbf{x}_{\alpha} = \Delta\mathbf{x}_{\alpha}$, $\mathbf{P}_{\mathbf{k}}\Delta\mathbf{x}'_{\alpha} = \Delta\mathbf{x}'_{\alpha}$, and $\mathbf{P}_{\mathbf{k}}\mathbf{k} = \mathbf{0}$, we have

$$2\Delta\mathbf{x}_{\alpha} - \lambda_{\alpha}\mathbf{P}_{\mathbf{k}}\mathbf{F}\mathbf{x}'_{\alpha} = \mathbf{0}, \quad 2\Delta\mathbf{x}'_{\alpha} - \lambda_{\alpha}\mathbf{P}_{\mathbf{k}}\mathbf{F}^{\top}\mathbf{x}_{\alpha} = \mathbf{0}. \quad (113)$$

Hence, we obtain

$$\Delta\mathbf{x}_{\alpha} = \frac{\lambda_{\alpha}}{2}\mathbf{P}_{\mathbf{k}}\mathbf{F}\mathbf{x}'_{\alpha}, \quad \Delta\mathbf{x}'_{\alpha} = \frac{\lambda_{\alpha}}{2}\mathbf{P}_{\mathbf{k}}\mathbf{F}^{\top}\mathbf{x}_{\alpha}. \quad (114)$$

Substituting these into (76), we have

$$\begin{aligned} & (\mathbf{F}\mathbf{x}'_{\alpha}, \frac{\lambda_{\alpha}}{2}\mathbf{P}_{\mathbf{k}}\mathbf{F}\mathbf{x}'_{\alpha}) + (\mathbf{F}^{\top}\mathbf{x}_{\alpha}, \frac{\lambda_{\alpha}}{2}\mathbf{P}_{\mathbf{k}}\mathbf{F}^{\top}\mathbf{x}_{\alpha}) \\ & = (\mathbf{x}_{\alpha}, \mathbf{F}\mathbf{x}'_{\alpha}), \end{aligned} \quad (115)$$

and hence

$$\frac{\lambda_{\alpha}}{2} = \frac{(\mathbf{x}_{\alpha}, \mathbf{F}\mathbf{x}'_{\alpha})}{(\mathbf{F}\mathbf{x}'_{\alpha}, \mathbf{P}_{\mathbf{k}}\mathbf{F}\mathbf{x}'_{\alpha}) + (\mathbf{F}^{\top}\mathbf{x}_{\alpha}, \mathbf{P}_{\mathbf{k}}\mathbf{F}^{\top}\mathbf{x}_{\alpha})}. \quad (116)$$

Substituting this into (114), we obtain (78). If we substitute (78) into (74), we have

$$\begin{aligned} E &= \sum_{\alpha=1}^N \left(\left\| \frac{(\mathbf{x}_{\alpha}, \mathbf{F}\mathbf{x}'_{\alpha})\mathbf{P}_{\mathbf{k}}\mathbf{F}\mathbf{x}'_{\alpha}}{(\mathbf{x}'_{\alpha}, \mathbf{F}^{\top}\mathbf{P}_{\mathbf{k}}\mathbf{F}\mathbf{x}'_{\alpha}) + (\mathbf{x}_{\alpha}, \mathbf{F}\mathbf{P}_{\mathbf{k}}\mathbf{F}^{\top}\mathbf{x}_{\alpha})} \right\|^2 \right. \\ & \quad \left. + \left\| \frac{(\mathbf{x}_{\alpha}, \mathbf{F}\mathbf{x}'_{\alpha})\mathbf{P}_{\mathbf{k}}\mathbf{F}^{\top}\mathbf{x}_{\alpha}}{(\mathbf{x}'_{\alpha}, \mathbf{F}^{\top}\mathbf{P}_{\mathbf{k}}\mathbf{F}\mathbf{x}'_{\alpha}) + (\mathbf{x}_{\alpha}, \mathbf{F}\mathbf{P}_{\mathbf{k}}\mathbf{F}^{\top}\mathbf{x}_{\alpha})} \right\|^2 \right) \\ &= \sum_{\alpha=1}^N \frac{(\mathbf{x}_{\alpha}, \mathbf{F}\mathbf{x}'_{\alpha})^2 (\|\mathbf{P}_{\mathbf{k}}\mathbf{F}\mathbf{x}'_{\alpha}\|^2 + \|\mathbf{P}_{\mathbf{k}}\mathbf{F}^{\top}\mathbf{x}_{\alpha}\|^2)}{\left((\mathbf{F}\mathbf{x}'_{\alpha}, \mathbf{P}_{\mathbf{k}}\mathbf{F}\mathbf{x}'_{\alpha}) + (\mathbf{F}^{\top}\mathbf{x}_{\alpha}, \mathbf{P}_{\mathbf{k}}\mathbf{F}^{\top}\mathbf{x}_{\alpha}) \right)^2} \\ &= \sum_{\alpha=1}^N \frac{(\mathbf{x}_{\alpha}, \mathbf{F}\mathbf{x}'_{\alpha})^2}{(\mathbf{F}\mathbf{x}'_{\alpha}, \mathbf{P}_{\mathbf{k}}\mathbf{F}\mathbf{x}'_{\alpha}) + (\mathbf{F}^{\top}\mathbf{x}_{\alpha}, \mathbf{P}_{\mathbf{k}}\mathbf{F}^{\top}\mathbf{x}_{\alpha})}, \end{aligned} \quad (117)$$

where we have noted due to the identity $\mathbf{P}_{\mathbf{k}}^2 = \mathbf{P}_{\mathbf{k}}$ that $\|\mathbf{P}_{\mathbf{k}}\mathbf{F}\mathbf{x}'_{\alpha}\|^2 = (\mathbf{P}_{\mathbf{k}}\mathbf{F}\mathbf{x}'_{\alpha}, \mathbf{P}_{\mathbf{k}}\mathbf{F}\mathbf{x}'_{\alpha}) = (\mathbf{F}\mathbf{x}'_{\alpha}, \mathbf{P}_{\mathbf{k}}^2\mathbf{F}\mathbf{x}'_{\alpha}) = (\mathbf{F}\mathbf{x}'_{\alpha}, \mathbf{P}_{\mathbf{k}}\mathbf{F}\mathbf{x}'_{\alpha})$. Similarly, we have $\|\mathbf{P}_{\mathbf{k}}\mathbf{F}^{\top}\mathbf{x}_{\alpha}\|^2 = (\mathbf{F}^{\top}\mathbf{x}_{\alpha}, \mathbf{P}_{\mathbf{k}}\mathbf{F}^{\top}\mathbf{x}_{\alpha})$.

Introducing Lagrange multipliers λ_{α} , μ_{α} , and μ'_{α} for the constraints of (85), and (87) to (74), we let

$$L = \sum_{\alpha=1}^N \left(\|\tilde{\mathbf{x}}_{\alpha} + \Delta\hat{\mathbf{x}}_{\alpha}\|^2 + \|\tilde{\mathbf{x}}'_{\alpha} + \Delta\hat{\mathbf{x}}'_{\alpha}\|^2 \right)$$

$$\begin{aligned} & - \sum_{\alpha=1}^N \lambda_{\alpha} \left((\mathbf{F}\hat{\mathbf{x}}'_{\alpha}, \Delta\hat{\mathbf{x}}_{\alpha}) + (\mathbf{F}^{\top}\hat{\mathbf{x}}_{\alpha}, \Delta\hat{\mathbf{x}}'_{\alpha}) \right) \\ & - \sum_{\alpha=1}^N \mu_{\alpha}(\mathbf{k}, \Delta\hat{\mathbf{x}}_{\alpha}) - \sum_{\alpha=1}^N \mu'_{\alpha}(\mathbf{k}, \Delta\hat{\mathbf{x}}'_{\alpha}). \end{aligned} \quad (118)$$

Letting the derivatives of L with respect to $\Delta\hat{\mathbf{x}}_{\alpha}$ and $\Delta\hat{\mathbf{x}}'_{\alpha}$ be $\mathbf{0}$, we have

$$\begin{aligned} 2(\tilde{\mathbf{x}}_{\alpha} + \Delta\hat{\mathbf{x}}_{\alpha}) - \lambda_{\alpha}\mathbf{F}\hat{\mathbf{x}}'_{\alpha} - \mu_{\alpha}\mathbf{k} &= \mathbf{0}, \\ 2(\tilde{\mathbf{x}}'_{\alpha} + \Delta\hat{\mathbf{x}}'_{\alpha}) - \lambda_{\alpha}\mathbf{F}^{\top}\hat{\mathbf{x}}_{\alpha} - \mu'_{\alpha}\mathbf{k} &= \mathbf{0}. \end{aligned} \quad (119)$$

Multiplying $\mathbf{P}_{\mathbf{k}}$ on both sides from left, we have

$$\begin{aligned} 2\tilde{\mathbf{x}}_{\alpha} + 2\Delta\hat{\mathbf{x}}_{\alpha} - \lambda_{\alpha}\mathbf{P}_{\mathbf{k}}\mathbf{F}\hat{\mathbf{x}}'_{\alpha} &= \mathbf{0}, \\ 2\tilde{\mathbf{x}}'_{\alpha} + 2\Delta\hat{\mathbf{x}}'_{\alpha} - \lambda_{\alpha}\mathbf{P}_{\mathbf{k}}\mathbf{F}^{\top}\hat{\mathbf{x}}_{\alpha} &= \mathbf{0}. \end{aligned} \quad (120)$$

Substituting these into (86), we have

$$\Delta\hat{\mathbf{x}}_{\alpha} = \frac{\lambda_{\alpha}}{2}\mathbf{P}_{\mathbf{k}}\mathbf{F}\hat{\mathbf{x}}'_{\alpha} - \tilde{\mathbf{x}}_{\alpha}, \quad \Delta\hat{\mathbf{x}}'_{\alpha} = \frac{\lambda_{\alpha}}{2}\mathbf{P}_{\mathbf{k}}\mathbf{F}^{\top}\hat{\mathbf{x}}_{\alpha} - \tilde{\mathbf{x}}'_{\alpha}. \quad (121)$$

Substituting these into (86), we obtain

$$\begin{aligned} & (\mathbf{F}\hat{\mathbf{x}}'_{\alpha}, \frac{\lambda_{\alpha}}{2}\mathbf{P}_{\mathbf{k}}\mathbf{F}\hat{\mathbf{x}}'_{\alpha} - \tilde{\mathbf{x}}_{\alpha}) \\ & + (\mathbf{F}^{\top}\hat{\mathbf{x}}_{\alpha}, \frac{\lambda_{\alpha}}{2}\mathbf{P}_{\mathbf{k}}\mathbf{F}^{\top}\hat{\mathbf{x}}_{\alpha} - \tilde{\mathbf{x}}'_{\alpha}) = (\hat{\mathbf{x}}_{\alpha}, \mathbf{F}\hat{\mathbf{x}}'_{\alpha}), \end{aligned} \quad (122)$$

and hence

$$\frac{\lambda_{\alpha}}{2} = \frac{(\hat{\mathbf{x}}_{\alpha}, \mathbf{F}\hat{\mathbf{x}}'_{\alpha}) + (\mathbf{F}\hat{\mathbf{x}}'_{\alpha}, \tilde{\mathbf{x}}_{\alpha}) + (\mathbf{F}^{\top}\hat{\mathbf{x}}_{\alpha}, \tilde{\mathbf{x}}'_{\alpha})}{(\mathbf{F}\hat{\mathbf{x}}'_{\alpha}, \mathbf{P}_{\mathbf{k}}\mathbf{F}\hat{\mathbf{x}}'_{\alpha}) + (\mathbf{F}^{\top}\hat{\mathbf{x}}_{\alpha}, \mathbf{P}_{\mathbf{k}}\mathbf{F}^{\top}\hat{\mathbf{x}}_{\alpha})}. \quad (123)$$

Substituting this into (121), we obtain (89). If we substitute (89) into (83), we have

$$\begin{aligned} E &= \sum_{\alpha=1}^N \left(\left\| \frac{(\hat{\mathbf{x}}_{\alpha}, \mathbf{F}\hat{\mathbf{x}}'_{\alpha}) + (\mathbf{F}\hat{\mathbf{x}}'_{\alpha}, \tilde{\mathbf{x}}_{\alpha}) + (\mathbf{F}^{\top}\hat{\mathbf{x}}_{\alpha}, \tilde{\mathbf{x}}'_{\alpha})}{(\mathbf{F}\hat{\mathbf{x}}'_{\alpha}, \mathbf{P}_{\mathbf{k}}\mathbf{F}\hat{\mathbf{x}}'_{\alpha}) + (\mathbf{F}^{\top}\hat{\mathbf{x}}_{\alpha}, \mathbf{P}_{\mathbf{k}}\mathbf{F}^{\top}\hat{\mathbf{x}}_{\alpha})} \mathbf{P}_{\mathbf{k}}\mathbf{F}\hat{\mathbf{x}}'_{\alpha} \right\|^2 \right. \\ & \quad \left. + \left\| \frac{(\hat{\mathbf{x}}_{\alpha}, \mathbf{F}\hat{\mathbf{x}}'_{\alpha}) + (\mathbf{F}\hat{\mathbf{x}}'_{\alpha}, \tilde{\mathbf{x}}_{\alpha}) + (\mathbf{F}^{\top}\hat{\mathbf{x}}_{\alpha}, \tilde{\mathbf{x}}'_{\alpha})}{(\mathbf{F}\hat{\mathbf{x}}'_{\alpha}, \mathbf{P}_{\mathbf{k}}\mathbf{F}\hat{\mathbf{x}}'_{\alpha}) + (\mathbf{F}^{\top}\hat{\mathbf{x}}_{\alpha}, \mathbf{P}_{\mathbf{k}}\mathbf{F}^{\top}\hat{\mathbf{x}}_{\alpha})} \mathbf{P}_{\mathbf{k}}\mathbf{F}^{\top}\hat{\mathbf{x}}_{\alpha} \right\|^2 \right) \\ &= \sum_{\alpha=1}^N \frac{\left((\hat{\mathbf{x}}_{\alpha}, \mathbf{F}\hat{\mathbf{x}}'_{\alpha}) + (\mathbf{F}\hat{\mathbf{x}}'_{\alpha}, \tilde{\mathbf{x}}_{\alpha}) + (\mathbf{F}^{\top}\hat{\mathbf{x}}_{\alpha}, \tilde{\mathbf{x}}'_{\alpha}) \right)^2}{\left((\mathbf{F}\hat{\mathbf{x}}'_{\alpha}, \mathbf{P}_{\mathbf{k}}\mathbf{F}\hat{\mathbf{x}}'_{\alpha}) + (\mathbf{F}^{\top}\hat{\mathbf{x}}_{\alpha}, \mathbf{P}_{\mathbf{k}}\mathbf{F}^{\top}\hat{\mathbf{x}}_{\alpha}) \right)^2} \\ & \quad \left(\|\mathbf{P}_{\mathbf{k}}\mathbf{F}\hat{\mathbf{x}}'_{\alpha}\|^2 + \|\mathbf{P}_{\mathbf{k}}\mathbf{F}^{\top}\hat{\mathbf{x}}_{\alpha}\|^2 \right) \\ &= \sum_{\alpha=1}^N \frac{\left((\hat{\mathbf{x}}_{\alpha}, \mathbf{F}\hat{\mathbf{x}}'_{\alpha}) + (\mathbf{F}\hat{\mathbf{x}}'_{\alpha}, \tilde{\mathbf{x}}_{\alpha}) + (\mathbf{F}^{\top}\hat{\mathbf{x}}_{\alpha}, \tilde{\mathbf{x}}'_{\alpha}) \right)^2}{\left((\mathbf{F}\hat{\mathbf{x}}'_{\alpha}, \mathbf{P}_{\mathbf{k}}\mathbf{F}\hat{\mathbf{x}}'_{\alpha}) + (\mathbf{F}^{\top}\hat{\mathbf{x}}_{\alpha}, \mathbf{P}_{\mathbf{k}}\mathbf{F}^{\top}\hat{\mathbf{x}}_{\alpha}) \right)}. \end{aligned} \quad (124)$$